1. Introduction

Colloidal carriers have been used for many years mainly as the modified formulation of drug molecules exhibiting low aqueous solubility. The discovery of new therapeutic agents has facilitated a demand for more sophisticated carrier systems which are able to protect agents from inactivation due to chemical or enzymatic degradation, migrate, and selectively accumulate at target sites in the body, thus enhancing the performance of the delivered agents. The recent progress in polymer science and nanotechnology certainly lends a strong basis to develop such colloidal carriers with high performance and modulated targetability.

Among these colloidal carriers, polymeric micelles have received significant attention as a promising supramolecular carrier system [1–5] due to their small size and stability, which lead to a prolonged blood circulation with reduced nonspecific accumulation in normal tissues and preferential accumulation in solid tumors by the enhanced permeability and retention (EPR) effect [6]. In addition to these exceptional properties, a high loading capacity of hydrophobic drug in the micelle core establishes polymeric micelle as a unique anticancer drug delivery system [7,8].

Previously, *cis*-dichlorodiammineplatinum(II) (cisplatin, CDDP; Fig. 1), a widely used anticancer drug, was incorporated into poly(ethylene glycol)–poly(amino acid) block copolymers [poly(aspartic acid) or poly(glutamic acid)] forming polymeric micelles [9]. The physicochemical and biological properties of this micelle were extensively studied [9–13], indicating that CDDP-loaded micelles are an effective delivery system for CDDP complexes.

CDDP shows acute dose-related side effects (such as nephrotoxicity, ototoxicity, neurotoxicity, nausea, vomiting, and mielosupression) and the appearance of intrinsic and acquired resistance [14]. Thus, since the discovery of CDDP in the mid-1960s, the enormous efforts to develop improved CDDP analogs had been devoted. Nevertheless, a limited number of these analogs reached their final approval. Among these compounds, dichloro(1,2-diaminocyclohexane)platinum(II) (DACHPt; Fig. 1) has shown wide and markedly different spectrum of activity than CDDP, such as lower toxicity than CDDP and no cross-resistance with CDDP in many CDDP-resistant

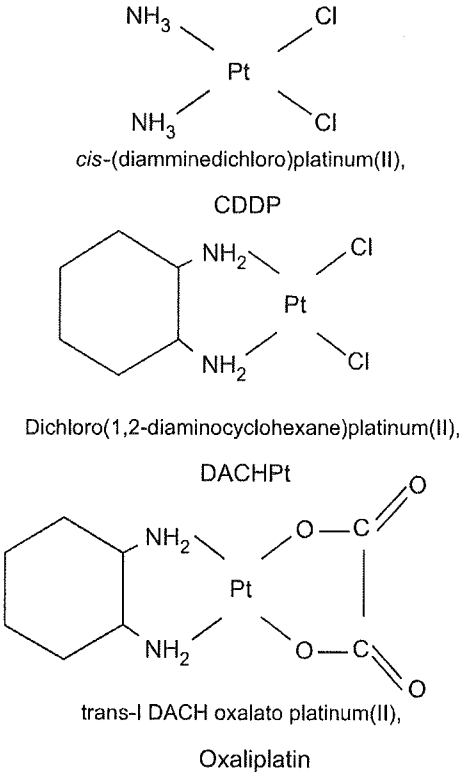

Fig. 1. Chemical structures of cisplatin, DACHPt, and oxaliplatin.

cancers [15–22]. However, the solubility of DACHPt in water is much lower than CDDP (0.25 mg/ml for DACHPt vs. 1.2 mg/ml for CDDP) [17]. With the purpose of enhancing water solubility of DACHPt, oxalate 1,2-diaminocyclohexane platinum(II) (oxaliplatin; Fig. 1) was develop by Kidani et al. in 1977 [16]. Oxaliplatin is a third generation platinum drug approved by the Food and Drug Administration (FDA) in the U.S.A. in 2002. Stability, solubility, formulation, and safety issues were more promising for oxaliplatin than for other diaminocyclohexane (DACH)-platinum compounds initially selected for preclinical testing and evaluated in early clinical trials. Oxaliplatin possesses an oxalate group, which is displaced by water and nucleophiles (such as Cl^- and HCO_3^- ions) in biological media to activate the drug, and it also has a nonhydrolysable diaminocyclohexane (DACH) ligand, which is maintained in the final active cytotoxic metabolites of the drug. From a pharmacological standpoint, the differential resistance of CDDP and oxaliplatin appears to be linked to the DACH ligand. This DACH ligand may induce DNA

lesions, which are poorly recognized by DNA recognition and repair pathways [23,24].

Although oxaliplatin shows better relative tolerability compared to other platinum compounds, a small number of side effects (like cumulative peripheral distal neurotoxicity and acute dysesthesias) restrain the range of working doses [25–28]. Recently, many drug delivery systems have been developed to increase oxaliplatin efficiency as well as to modify its pharmacokinetics. These drug delivery systems

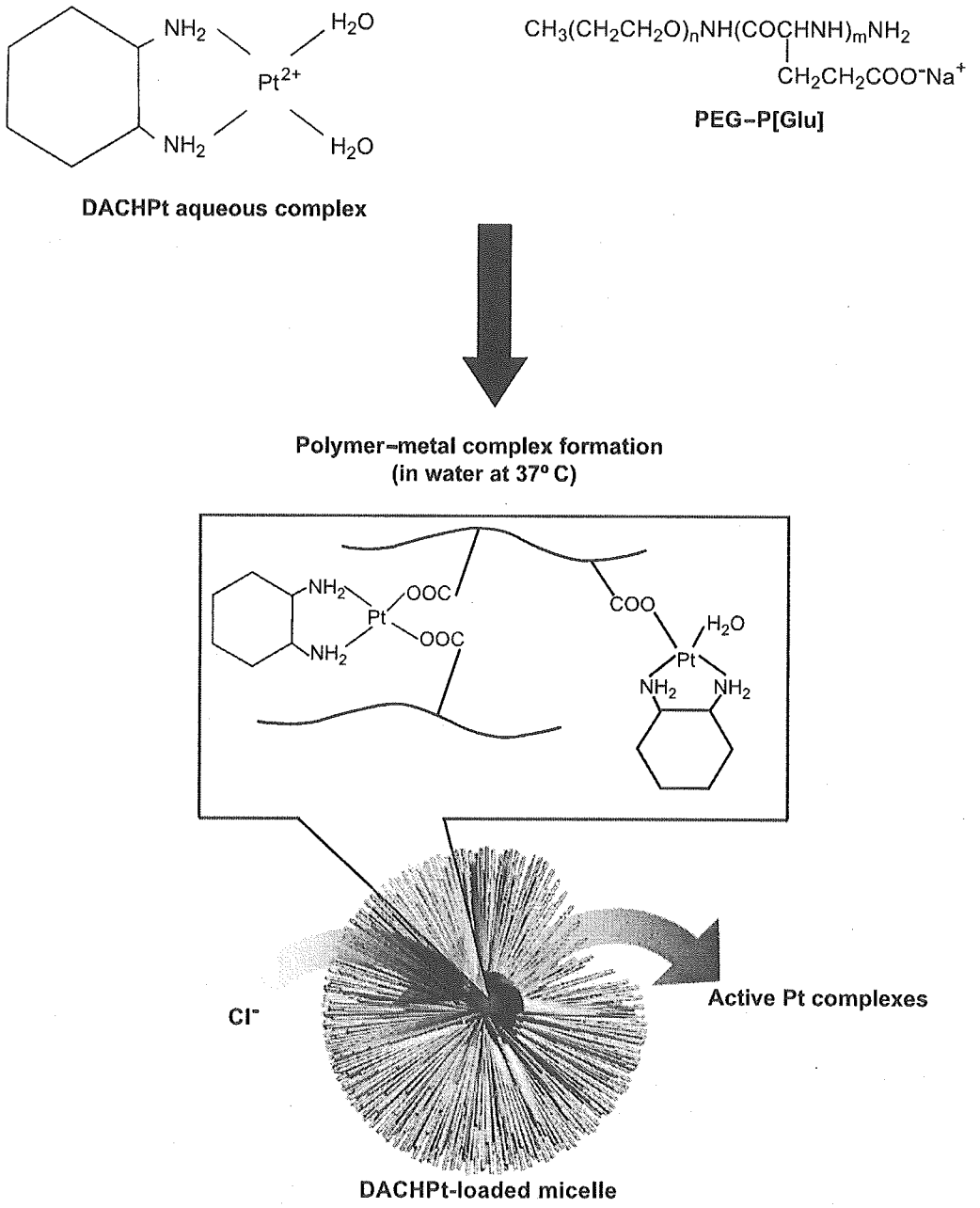

Fig. 2. Preparation of DACHPt-loaded micelles and release of drug in media containing chloride ion.

include microspheres [29], stealth liposomes [30], and macromolecular drugs [31]. The development of polymeric micelles loaded with DACHPt could lead to an oxaliplatin carrier with superior properties such as prolonged blood circulation or higher tumor accumulation. Thus, in the present study, novel polymeric micelles entrapping DACHPt in their core were prepared through the polymer–metal complex formation between DACHPt and poly(ethylene glycol)–poly(glutamic acid) block copolymers [PEG–P(Glu)] in distilled water after converting DACHPt to its aqueous complex by pretreatment with $AgNO_3$ (Fig. 2) to increase water solubility. Subsequently, the biological properties of DACHPt-loaded micelles were characterized. The kinetic stability of the carrier as well as the release rate of platinum complexes from the micelle core were evaluated in phosphate buffered saline solution. Moreover, in vivo experiments were performed on tumor-bearing mice to study the plasma clearance and the tumor accumulation of DACHPt-loaded micelles and free oxaliplatin. Finally, the in vitro cytotoxicity against murine colon carcinoma cell line was evaluated to compare the cytotoxicity of the DACHPt micellar system with that of free oxaliplatin.

2. Materials and methods

2.1. Materials

β-Benzyl L-glutamate was bought from Sigma Chemical (St. Louis, MO). Bis(trichloromethyl)carbonate (triphosgene) was purchased from Tokyo Kasei Kogyo (Tokyo, Japan). *N*,*N*-Dimethylformamide (DMF) and 3-(4,5-dimethylthiazol-2-yl)-2,5-diphenyltetrazolium bromide (MTT) were obtained from Wako Pure Chemical (Osaka, Japan). Dichloro(1,2-diamminocyclohexane)platinum(II) (DACHPt) and $AgNO_3$ were purchased from Aldrich Chemical (Milwaukee, WI). α-Methoxy-ω-aminopoly(ethylene glycol) (CH_3O-PEG-NH_2; M_w=12,000) was purchased from Nippon Oil and Fats (Tokyo, Japan). Murine colon adenocarcinoma 26 (C-26) cells were kindly supplied from the National Cancer Center (Tokyo, Japan). C-26 cells were maintained in RPMI 1640 medium (Sigma Chemical) containing 10% fetal bovine serum in a humidified atmosphere containing 5% CO_2 at 37 °C.

2.2. Preparation of PEG–P(Glu)

PEG–P(Glu) block copolymers were synthesized according to the previously described synthetic method of PEG–P(Asp) [9] with a slight modification. Briefly, the *N*-carboxy anhydride of γ-benzyl L-glutamate was synthesized by the Fuchs–Farthing method, using triphosgene. Then, *N*-carboxy anhydride of γ-benzyl L-glutamate was polymerized in DMF, initiated by the primary amino group of CH_3O–PEG–NH_2, to obtain PEG–poly(γ-benzyl L-glutamate) (PEG–PBLG) block copolymer. A narrow distribution (M_w/M_n: 1.06) of PEG–PBLG was confirmed by gel permeation chromatography [column: TSK-gel G3000HHR, G4000HHR (Tosoh, Yamaguchi, Japan); eluent: DMF containing 10 mM LiCl; flow rate: 0.8 ml/min; detector: refractive index (RI); temperature: 25 °C]. The polymerization degree of PBLG was determined to be 46 by comparing the proton ratios of methylene units in PEG (-OCH_2CH_2-: δ=3.7 ppm) and phenyl groups of PBLG (-$CH_2C_6H_5$: δ=7.3 ppm) in ^{1}H-NMR measurement [JEOL EX270 (JEOL, Tokyo, Japan) solvent: DMSO-d_6; temperature: 80 °C]. The deprotection of the benzyl group of PEG–PBLG was carried out by mixing with 0.5 N NaOH at room temperature to obtain PEG–P(Glu).

2.3. Preparation of DACHPt-loaded micelles

DACHPt (5 mM) was suspended in distilled water and mixed with silver nitrate ([$AgNO_3$]/[DACHPt]=1) to form the aqueous complex (Fig. 2). The solution was kept in dark at 25 °C for 24 h. AgCl precipitates were found after reaction. Next, the mixture was centrifuged at 3000 rpm for 10 min to eliminate the AgCl precipitates. Afterward, the supernatant was purified by passage through a 0.22-μm filter.

PEG–P(Glu) was added to the solution of DACHPt aqueous complex (polymer concentration: 2.1 mg/ml; [Glu]=5 mmol/liter; [DACHPt]/[Glu]=1.0) and reacted for 120 h to prepare DACHPt-loaded micelles. The prepared micelles were purified by ultrafiltration [molecular weight cutoff size (MWCO): 100,000]. The size distribution of DACHPt-loaded micelles was evaluated by dynamic light scattering (DLS) measurement at 25 °C using a Photal dynamic laser scattering spectrometer DLS-7000 (Otsuka Electronics, Osaka,

Japan). The Pt content in the micelles was determined by ion coupled plasma-mass spectrometry (ICP-MS, Hewlett Packard 4500).

2.4. Drug release in phosphate buffered saline

The release of the platinum from the micelles in phosphate buffered saline at 37 °C was evaluated by the dialysis method [Spectra/Por-6 (MWCO: 1000), Spectrum Laboratories, Rancho Dominguez, CA]. Briefly, a micellar solution of known platinum drug concentration was placed inside a dialysis bag and dialyzed against phosphate buffered saline (10 mM phosphate buffer, pH 7.4, plus 150 mM NaCl) at 37 °C. The released Pt outside of the dialysis bag was sampled at defined time periods and measured by ICP-MS.

2.5. Micellar kinetic stability in phosphate buffered saline

The kinetic stability of DACHPt-loaded micelles in phosphate buffered saline at 37 °C was evaluated by static light scattering measurement using a DLS-7000, according to the method reported previously [9]. Changes in the scattering light intensity (i.e., the Rayleigh ratio at 90° of the scattering angle) were measured at a defined time period. In this analysis, a decrease in the scattering light intensity is due to a decrease in the apparent molecular weight of the micelles as well as in the micelle concentration.

2.6. Platinum concentration in plasma and platinum accumulation in tumor

CDF_1 mice (female, n=6) were inoculated subcutaneously with C-26 cells (1×10^6). After 14 days, oxaliplatin and DACHPt-loaded micelles were administered i.v. at a dose of 100 μg/mouse on a platinum basis (tumor weight: 0.2±0.05 g; mean±S.D.). The mice were sacrificed after defined time periods (1, 5, 9, 27, 48, and 72 h). The tumor was excised, and the blood was collected from the inferior vena cava, heparinized, and centrifuged to obtain the plasma. The plasma and the tumor were decomposed on heating in nitric acid, evaporated to dryness, and redissolved in 2 N hydrochloric acid solution. The Pt concentration in the solution was measured by ICP-MS.

2.7. In vitro cytotoxicity

Fifty percent growth inhibitory concentration (IC_{50}) of free oxaliplatin and DACHPt-loaded micelles on the C-26 cell lines was evaluated by MTT assay. C-26 cells (5000 cells) were cultured in RPMI 1640 containing 10% fetal bovine serum in a 96-well multiplate. Then, the cells were exposed to free oxaliplatin or DACHPt-loaded micelles for 48 or 72 h, and MTT solution was added. Cell viability was measured by the formed formazan absorbance at 570 nm.

3. Results and discussion

3.1. Micelle size and size distribution

The driving force for micelle assembly is the metal–polymer complex formation between the platinum of DACHPt and the carboxylic group of the P(Glu), as seen in Fig. 2 [9]. Once the micelles were formed, free platinum complexes and block copolymer were eliminated by dialysis and ultrafiltration. After micelles purification, the cumulant diameter of DACHPt-loaded micelles was measured by dynamic light scattering measurements. The size was determined to be 40 nm for the micelle prepared at [DACHPt]/[Glu]=0.75 with a considerable low cumulant polydispersity (μ_2/T^2=0.03). Note that the size of a colloidal drug carrier is a determinant feature of its fate in blood circulation and its biodistribution. The recognition by the reticuloendothelial system (RES) is known to be the principal reason for the removal of many colloidal drug carriers from the blood compartment. The size of a colloidal carrier is favorable to be below 200 nm, and its optimization may result in the extension of blood circulation. The sub-100 nm size as well as the hydrophilic PEG palisade surrounding the core are the substantial advantages of the micelles to avoid their uptake by the RES. Solid tumors display diverse pore cutoff size for transvascular transport, depending on the microenvironment and on their type [32–34]. Therefore, the dimension of a drug carrier critically affects its extravasation efficiency, and this efficiency varies for different tumors. Nevertheless, the size of the micelles (40 nm) is small enough to reasonably assume a high extravasation efficiency

regardless of the tumor type and conditions [32,33]. Also, it has been reported that small sized carriers with sizes under 100 nm can attain deeper penetration into poorly permeable tumors, and consequently, increased accumulation [35]. Thus, the size of DACHPt-loaded micelles appears to be optimal from the standpoint of tumor-targeted therapy.

The yield of platinum loading was 75% of the initial feed amount at [DACHPt]/[Glu]=0.75. However, it could be increased by augmenting the [DACHPt]/[Glu] molar ratio, as seen in Fig. 3, obtaining approximately 90% incorporation of fed drug. The size of the micelles could also be changed by the incorporation amount of drug to the poly(-glutamic acid) backbone. Fig. 4 shows a change in the cumulant diameter for DACHPt-loaded micelles against [DACHPt]/[Glu] molar ratio. The size ranged from 25 nm for a [DACHPt]/[Glu] molar ratio equal to 0.25 to 50 nm for a [DACHPt]/[Glu] molar ratio equal to 1.5. Here, the simple size control with narrow distribution in polymeric micelles is a unique attribute that may not be seen in other colloidal carriers.

3.2. Release of DACHPt complexes

In the case of physically encapsulated drugs in polymeric micelles, the release rate is controlled by diffusion out of the micellar core or by the disintegration of the micelles. On the other hand, when the drug and the polymer form conjugates, the bond between them has to be cleaved for drug release [36,37]. Thus, in chemically conjugated polymeric micelles, the

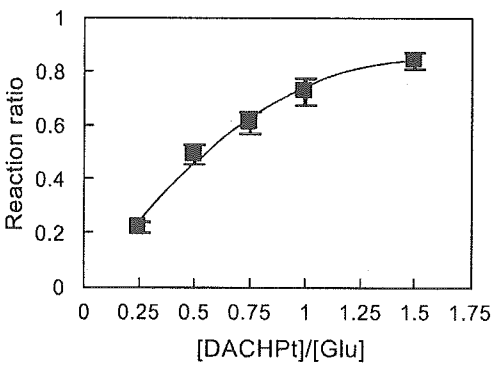

Fig. 3. Effect of [DACHPt]/[Glu] feeding molar ratios on the reaction ratio of Glu units in the block copolymer with DACHPt. Data are shown as the mean±S.D. (n=3).

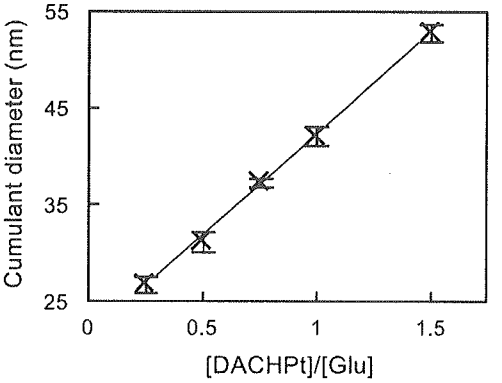

Fig. 4. Change in micelle size due to the variation of the [DACHPt]/[Glu] molar ratio measured by DLS at 25 °C. Data are shown as the mean±S.D. (n=3).

mechanism for drug release can be summarized in three steps: initially, the molecules that activate the bond cleavage penetrate into the micelle core; next, the cleavage of the bonds between drug and polymer occurs; and finally, the drug diffuses out of the micelle. Additionally, if the micellar structure is sufficiently stable, drug release could even be delayed until the carrier reaches the target. The premature drug release from the carrier is an undesired event, which can lead to toxic effects due to the presence of free drug in the blood stream.

DACHPt-loaded micelles did not show any release of platinum complexes in distilled water (data not shown). However, in media containing chloride ions, platinum complexes could be released from the micelle core by exchange reaction between chloride ions and carboxylic groups of P(Glu) in the platinum complexes (Fig. 2). The release profile of platinum complexes from the DACHPt-loaded micelles is shown in Fig. 5. During the first 15 h of exposure, the micelles presented an induction period. This phase may be related to the hydrophobic nature of the core of DACHPt-loaded micelles, which may hamper the in/out diffusion of water, ions, and Pt. After the induction period, the micelles released the drug in a sustained way, and the release rate of DACHPt-loaded micelle was found to be similar to that of CDDP-loaded micelles [13]. Probably, after the induction period, enough amount of DACHPt–P(Glu) complexes has been cleaved by the chloride ions to augment the hydrophilicity of the micelle core and to facilitate the diffusion out of platinum complexes.

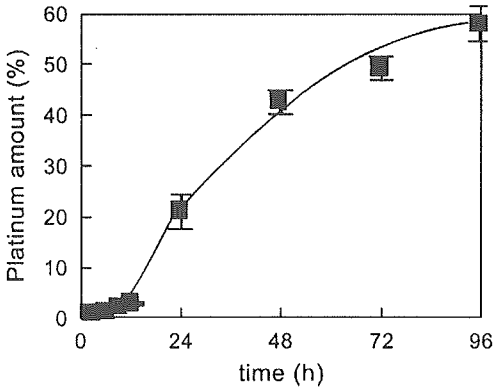

Fig. 5. Release profile of DACHPt from the micelles in phosphate buffered saline (pH 7.4) at 37 °C. The amount of platinum in the solutions was measured by ICP-MS. Data are shown as the mean±S.D. (n=4).

This unique profile of drug release owing to the induction period may still be rare in the other drug delivery systems for oxaliplatin active complexes [29,31] and might be advantageous for in vivo use because drug release is expected to be accelerated after the micelles reach the site of tumor.

3.3. Micelle kinetic stability

The kinetic stability of the micelle was measured by static light scattering. A decrease in the relative scattering intensity was considered to be owing to micellar disruption. The average diameter of the micelles was measured by DLS at the same time. The changes in the relative scattering intensity and the cumulant diameter of the micelle in phosphate buffered saline at 37 °C are shown in Fig. 6.

Inasmuch as the driving force of the formation of CDDP-loaded and DACHPt-loaded micelles is the polymer-metal complex formation, the release of platinum complexes may destabilize the micelle structure. Indeed, we previously reported that CDDP-loaded micelles were detected by DLS only for 50 h in phosphate buffer saline at 37° [13]. On the other hand, the stability of the DACHPt-loaded micelles was significantly elevated, and the size was maintained for 240 h, whereas the DACHPt-loaded micelles showed a comparable release rate to CDDP-loaded micelles (Fig. 5). This elevated stability of DACHPt-loaded micelles might be due to the bulky and hydrophobic nature of the DACH group in DACHPt [38]. Thus, once the micelle is formed, the higher hydrophobicity of the micellar core might lead to an increased kinetic stability, maintaining the micelles form for prolonged time period.

The elevated stability in biological media is a desired property of drug carriers because it is correlated with longer blood circulation; however, in many cases, increasing the stability of the carrier could signify diminishing or impeding the drug release. On the other hand, DACHPt-loaded micelles

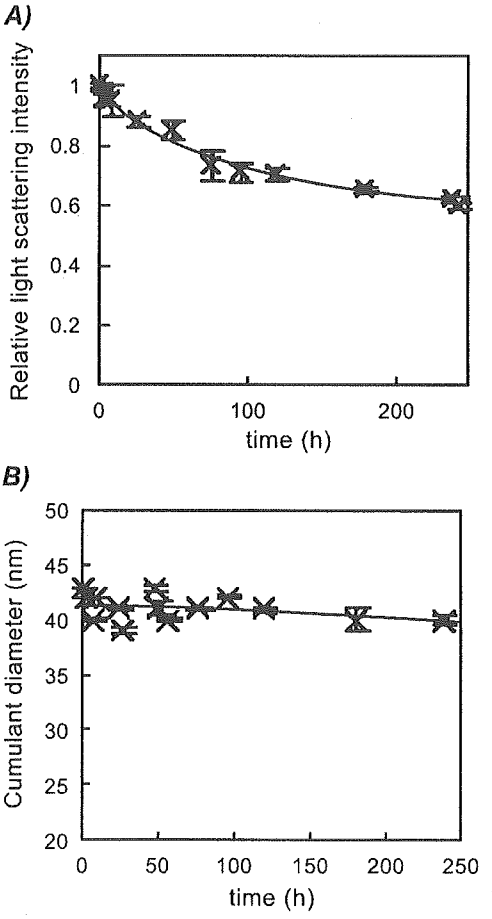

Fig. 6. Kinetic stability of DACHPt-loaded micelles in phosphate buffered saline at 37 °C. (A) Variation in the relative light scattering intensity of micellar solution (micelle concentration: 1.5 mg/ml) measured by SLS at a detection angle of 90° (phosphate buffered saline, 37 °C, pH 7.4). (B) Variation in the hydrodynamic diameter of micelle measured by cumulant approach of DLS. Data are shown as the mean±S.D. (n=3).

achieved high kinetic stability, which seems to be appropriate for systemic drug delivery, although the drug release from the micelles was not compromised.

3.4. Plasma clearance

Oxaliplatin elimination is mostly due to renal clearance. In clinical studies, it was observed that, at the end of a 2-h infusion of oxaliplatin, only 15% of the administered platinum was present in the systemic circulation. The plasma protein binding of platinum is irreversible, leading to inactivation of oxaliplatin, and is greater than 90%. Moreover, platinum binds irreversibly and accumulates in erythrocytes where it appears to have no relevant activity [22]. Thus, polymer conjugation of oxaliplatin will improve its blood circulation.

The platinum level in plasma after i.v. administration of free oxaliplatin or DACHPt-loaded micelles is shown in Fig. 7A. The DACHPt-loaded micelles showed remarkably prolonged blood circulation, whereas free oxaliplatin was cleared rapidly from circulation. Taking into account that the plasma volume in mice is 45.6 ml/kg [39], the platinum amount at 9 h for DACHPt-loaded micelle was determined to be over 80% of the injected dose and more than 16% even at 27 h after injection. We previously reported that CDDP-loaded micelles exhibited approximately 60% of the injected dose in plasma at 8 h and 13% of the injected dose at 24 h after injection [13]. The plasma Pt level of the micelles was appreciably augmented in the case of DACHPt-loaded micelles. It seems that the increased residence time of DACHPt-loaded micelles in the bloodstream is reasonably associated with the high kinetic stability of the micelles in phosphate buffered saline at 37 °C shown in Fig. 6.

3.5. Platinum accumulation in tumor

Selective and high accumulation of drug carriers at the tumor site is indispensable for drug targeting success. Accumulation of free oxaliplatin and DACHPt-loaded micelles in the solid tumor (C-26 cells) is shown in Fig. 7B. DACHPt-loaded micelles showed high and extended platinum levels at the tumor. Previously, we reported for CDDP-loaded micelles that the accumulation at tumor tissue took

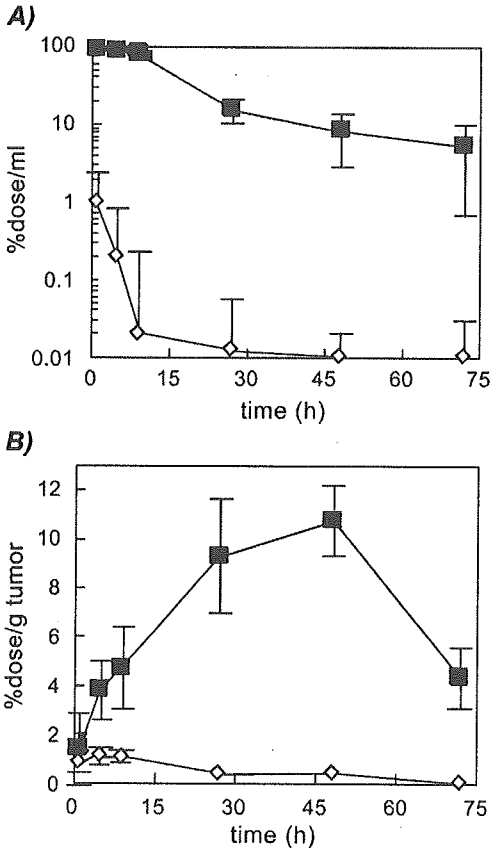

Fig. 7. Time profiles of platinum concentration in the plasma (A) and platinum accumulation in tumor (B) after i.v. administration of free oxaliplatin (◇) and DACHPt-loaded micelles (■). Each drug was administered to C-26-bearing CDF_1 mice (female, n=6) at a dose of 100 μg on Pt basis. Data are shown as the mean±S.D. (n=6).

maximum at 24 h with approximately 10% of the dose/g of tissue, and at that time, the platinum concentration in the blood was lower than 13% [13]. In the case of DACHPt-loaded micelles, the accumulation at the tumor at 24 h was similar to CDDP-loaded micelles. However, the former kept higher platinum concentration in plasma than the latter at the similar time range. Eventually, the maximum accumulation of DACHPt-loaded micelles was shifted to 48 h with 11% of the dose/g of tissue.

3.6. In vitro cytotoxicity

IC_{50} values are listed in Table 1 for DACHPt-loaded micelles and free oxaliplatin but also for CDDP-loaded micelles and free CDDP. Cytotoxicity

Table 1
In vitro cytotoxicity of free oxaliplatin, DACHPt-loaded micelles, free CDDP, and CDDP-loaded micelles against C-26 cell line

Incubation time (h)	IC_{50} (μM)[a]			
	Free oxaliplatin	DACHPt-loaded micelles	Free CDDP [12]	CDDP-loaded micelles [13]
48	8×10^{-4}	6×10^{-3}	8×10^{-3}	7×10^{-2}
72	2×10^{-4}	2×10^{-3}	2×10^{-3}	2×10^{-2}

[a] IC_{50} value obtained by 3-(4,5-dimethylthiazol-2-yl)-2,5-diphenyltetrazolium bromide assay.

of DACHPt-loaded micelles was approximately one order of magnitude lower than that observed for oxaliplatin, probably due to the slow release behavior of DACHPt complexes from the micelles. Nevertheless, DACHPt-loaded micelles showed comparable cytotoxicity to free CDDP and approximately 10 times higher than CDDP-loaded micelles [13] because DACHPt complexes are known to be much more cytotoxic than CDDP complexes [17]. This increased in vitro cytotoxicity of DACHPt-loaded micelles compared to CDDP-loaded micelles is promising for its in vivo application, considering that even the latter had an appreciable efficacy to cure solid tumors in experimental animals [13].

4. Conclusion

DACHPt-loaded micelles showed a size of 40 nm, which might be small enough to achieve extended blood circulation avoiding the uptake by the RES and to overcome the permeation barrier of poorly permeable tumors. DACHPt-loaded micelles showed considerable high stability, maintaining the size for 240 h in phosphate buffered saline, due to the highly hydrophobic core. Nevertheless, after an induction period of 15 h, the DACHPt complexes contained in the micelle core were released in a sustained way. In line with this release profile, the in vitro cytotoxicity assay against the C-26 cell line showed an appreciably lowered IC_{50} value after a prolonged incubation period of 72 h to expect high therapeutic index. Furthermore, prolonged blood circulation and increased tumor accumulation of DACHPt-loaded micelles compared to oxaliplatin were observed, facilitating their in vivo cytotoxicity against solid tumor, and a research in this direction is in progress in our laboratory.

Acknowledgement

This research was supported by the Special Coordination Funds for Promoting Science and Technology from the Ministry of Education, Culture, Sports, Science and Technology of Japan as well as by the Core Research Program for Evolutional Science and Technology (CREST) from Japan Science and Technology (JST).

References

[1] A.V. Kabanov, V.P. Chekhonin, V.Yu. Alakhov, E.V. Batrakova, A.S. Lebedev, N.S. Melik-Nubarov, S.A. Arzhakov, A.V. Levashov, G.V. Morozov, E.S. Severin, V.A. Kabanov, The neuroleptic activity of haloperidol increases after its solubilization in surfactant micelles: micelles as microcontainers for drug targeting, FEBS Lett. 258 (1989) 343–345.
[2] M. Yokoyama, M. Miyauchi, N. Yamada, T. Okano, Y. Sakurai, K. Kataoka, S. Inoue, Polymer micelles as novel drug carrier: adriamycin-conjugated poly(ethylene glycol)–poly(aspartic acid) block copolymer, J. Control. Release 11 (1990) 269–278.
[3] K. Kataoka, G.S. Kwon, M. Yokoyama, Y. Sakurai, T. Okano, Block copolymer micelles as vehicles for drug delivery, J. Control. Release 24 (1993) 119–132.
[4] C. Allen, D. Mysinger, A. Eisenberg, Nano-engineering block copolymer aggregates for drug delivery, Colloids Surf., B Biointerfaces 16 (1999) 3–27.
[5] K. Kataoka, A. Harada, Y. Nagasaki, Block copolymer micelles for drug delivery: design, characterization and biological significance, Adv. Drug Deliv. Rev. 47 (2001) 113–131.
[6] Y. Matsumura, H. Maeda, A new concept for macromolecular therapeutics in cancer chemotherapy: mechanism of tumoritropic accumulation of proteins and the antitumor agent SMANCS, Cancer Res. 46 (1986) 6387–6392.
[7] G.S. Kwon, M. Naito, M. Yokoyama, T. Okano, Y. Sakurai, K. Kataoka, Physical entrapment of adriamycin in AB block copolymer micelles, Pharm. Res. 12 (1995) 192–195.
[8] K. Kataoka, T. Matsumoto, M. Yokoyama, T. Okano, Y. Sakurai, S. Fukushima, K. Okamoto, G.S. Kwon, Doxorubicin-loaded poly(ethylene glycol)–poly(β-benzyl-L-aspartate) copolymer micelles: their pharmaceutical characteristics and biological significance, J. Control. Release 64 (2000) 143–153.
[9] N. Nishiyama, M. Yokoyama, T. Aoyagi, T. Okano, Y. Sakurai, K. Kataoka, Preparation and characterization of self-assembled polymer–metal complex micelle from *cis*-dichlorodiammineplatinum(II) and poly(ethylene glycol)–pol-

y(α,β-aspartic acid) block copolymer in an aqueous medium, Langmuir 15 (1999) 377–383.
[10] N. Nishiyama, K. Kataoka, Preparation and characterization of size-controlled polymeric micelle containing *cis*-dichlorodiammineplatinum(II) in the core, J. Control. Release 74 (2001) 83–94.
[11] Y. Mizumura, Y. Matsumura, T. Hamaguchi, N. Nishiyama, K. Kataoka, T. Kawaguchi, W.J.M. Hrushesky, F. Moriyasu, T. Kakizoe, Cisplatin-incorporated polymeric micelles eliminate nephrotoxicity, while maintaining antitumor activity, Jpn. J. Cancer Res. 92 (2001) 328–336.
[12] N. Nishiyama, Y. Kato, Y. Sugiyama, K. Kataoka, Cisplatin-loaded polymer–metal complex micelle with time-modulated decaying property as a novel drug delivery system, Pharm. Res. 18 (2001) 1035–1041.
[13] N. Nishiyama, S. Okazaki, H. Cabral, M. Miyamoto, Y. Kato, Y. Sugiyama, K. Nishio, Y. Matsumura, K. Kataoka, Novel cisplatin-incorporated polymeric micelles can eradicate solid tumors in mice, Cancer Res. 63 (2003) 8977–8983.
[14] B.A. Chabner, C.E. Myers, in: V.T. DeVita, S. Hellman, S.A. Rosenberg (Eds.), Cancer: Principles and Practice of Oncology, 3rd ed., JB Lippincott, Philadelphia, 1989.
[15] T.A. Connors, M. Jones, W.C. Ross, P.D. Braddock, A.R. Khokhar, M.L. Lobe, New platinum complexes with anti-tumor activity, Chem.-Biol. Interact. 5 (1972) 415–424.
[16] Y. Kidani, K. Inagaki, R. Saito, S. Tsukagoshi, Synthesis and anti-tumor activities of platinum(II) complexes of 1,2-diaminocyclohexane isomers and their related derivatives, J. Clin. Hematol. Oncol. 7 (1977) 197–202.
[17] Y. Kidani, M. Iigo, K. Inagaki, A. Hoshi, K. Kuretani, Antitumor activity of 1,2-diaminocyclohexane-platinum complexes against sarcoma-180 ascites form, J. Med. Chem. 21 (1978) 1315–1318.
[18] Y. Kidani, M. Noji, T. Tashiro, Antitumor activity of platinum(II) of 1,2-diaminocyclohexane isomers, Gann 71 (1980) 637–643.
[19] O. Rixe, W. Ortuzar, M. Alvarez, R. Parker, E. Reed, K. Paull, T. Fojo, Oxaliplatin, tetraplatin, cisplatin and carboplatin: spectrum of activity in drug resistant cell lines and in the cell lines of the national cancer institute's anticancer screen panel, Biochem. Pharmacol. 52 (1996) 1855–1865.
[20] C.X. Zhang, S.J. Lippard, New metal complexes as potential therapeutics, Curr. Opin. Chem. Biol. 7 (2003) 1–9.
[21] M. Karatalou, J.M. Essigmann, Mechanisms of resistance to cisplatin, Mutat. Res. 478 (2001) 23–43.
[22] M.A. Graham, G.F. Lockwood, D. Greensdale, S. Brieza, M. Bayssas, E. Gamelin, Clinical pharmacokinetics of oxaliplatin: a critical review, Clin. Cancer Res. 6 (2000) 1205–1218.
[23] E. Raymond, S. Faivre, S. Chaney, J. Woynarowski, E. Cvitkovic, Cellular and molecular pharmacology of oxaliplatin, Mol. Cancer Ther. 1 (2002) 227–235.
[24] A.M. Di Francesco, A. Ruggiero, R. Riccardi, Cellular and molecular aspects of drugs of the future: oxaliplatin, Cell. Mol. Life Sci. 59 (2002) 1914–1927.
[25] J.L. Misset, H. Bleiberg, W. Shuterland, Oxaliplatin clinical activity: a review, Crit. Rev. Oncol./Hematol. 35 (2000) 75–93.
[26] S. Giachetti, B. Perpoint, R. Zidani, Phase III multicenter randomized trial of oxaliplatin added to chronomodulated fluorouracil-leucovorin as first line treatment of metastasic colorectal cancer, J. Clin. Oncol. 18 (2000) 136–147.
[27] J.M. Extra, M. Espie, F. Calvo, Phase I study of oxaliplatin in patients with advanced cancer, Cancer Chemother. Pharmacol. 25 (1990) 299–303.
[28] G. Mathé, Y. Kidani, M. Segiguchi, M. Eriguchi, G. Fredj, G. Peytavin, J.L. Misset, S. Brienza, F. de Vassals, E. Chenu, C. Bourut, Oxalato-platinum or l-OHP, a third generation platinum complex: an experimental and clinical appraisal and preliminary comparison with *cis*-platinum and carboplatinum, Biomed. Pharmacother. 43 (1989) 237–250.
[29] F. Lagarce, O. Cruaud, C. Deuschel, M. Bayssas, G. Griffon-Etienne, J.P. Benoit, Oxaliplatin loaded PLAGA microspheres: design of specific release profiles, Int. J. Pharm. 242 (2002) 243–246.
[30] I. Han, O.J. Kim, G.Y. Lee, Y.K. Sung, R. Song, Y.S. Sohn, Enhanced antitumor activity of *trans*(±)-1,2-diaminocyclohexane glutamatoplatinum(II) with stealth liposome, Bioorganic Med. Chem. 11 (2003) 5443–5447.
[31] A. Furin, A. Guiotto, F. Baccicheti, G. Pasut, C. Deuschel, R. Bertani, F.M. Veronese, Synthesis, characterization and preliminary cytotoxicity assays of poly(ethylene glycol)-malonato-Pt-DACH conjugates, Eur. J. Med. Chem. 38 (2003) 739–749.
[32] V. Weissig, K.R. Whiteman, V.P. Torchilin, Accumulation of protein-loaded long circulating micelles and liposomes in subcutaneous lewis lung carcinoma, Pharm. Res. 15 (1998) 1552–1556.
[33] S.K. Hobbs, W.L. Monsky, F. Yuan, W.G. Roberts, L. Griffith, V.P. Torchilin, R.K. Jain, Regulation of transport pathways in tumor vessels: role of tumor type and microenvironment, Proc. Natl. Acad. Sci. U. S. A. 95 (1998) 4607–4612.
[34] O. Ishida, K. Maruyama, K. Sasaki, M. Iwatsuru, Size-dependent extravasation and interstitial localization of polyethyleneglycol liposomes in solid tumor-bearing mice, Int. J. Pharm. 190 (1999) 49–56.
[35] A. Lukyanov, Z. Gao, L. Mazzola, V.P. Torchilin, Polyethylene glycol-dyacyllipid micelles demonstrate increased accumulation in subcutaneous tumors in mice, Pharm. Res. 19 (2002) 1424–1429.
[36] C. Allen, D. Maysinger, A. Eisenberg, Nano-engineering block copolymer aggregates for drug delivery, Colloids Surf., B Biointerfaces 16 (1999) 3–27.
[37] A. Lavasanifar, J. Samuel, G.S. Kwon, Poly(ethylene oxide)-block-poly(L-amino acid) micelles for drug delivery, Adv. Drug Deliv. Rev. 54 (2002) 169–190.
[38] J.A. Platts, D.E. Hibbs, T.W. Hambley, M.D. Hall, Calculation of the hydrophobicity of platinum drugs, J. Med. Chem. 44 (2000) 472–474.
[39] F.G. King, R.L. Dedrick, Physiological pharmacokinetic parameters for *cis*-dichlorodiammineplatinum(II) (CDDP) in mouse, J. Pharmacokinet. Biopharm. 20 (1992) 95–99.

ugust 23, 2005 | vol. 102 | no. 34 | pp. 12177–12182

PNAS

roceedings of the National Academy of Sciences of the United States of America www.pnas.org

Efficient delivery of small interfering RNA to bone-metastatic tumors by using atelocollagen *in vivo*

Fumitaka Takeshita, Yoshiko Minakuchi, Shunji Nagahara, Kimi Honma, Hideo Sasaki, Kotaro Hirai, Takumi Teratani, Nachi Namatame, Yusuke Yamamoto, Koji Hanai, Takashi Kato, Akihiko Sano, and Takahiro Ochiya

Efficient delivery of small interfering RNA to bone-metastatic tumors by using atelocollagen *in vivo*

Fumitaka Takeshita*, Yoshiko Minakuchi†, Shunji Nagahara†, Kimi Honma‡, Hideo Sasaki*, Kotaro Hirai*, Takumi Teratani*, Nachi Namatame§, Yusuke Yamamoto§, Koji Hanai†, Takashi Kato§, Akihiko Sano†, and Takahiro Ochiya*¶

*Section for Studies on Metastasis, National Cancer Center Research Institute, Tokyo 104-0045, Japan; †Formulation Research Laboratories, Sumitomo Pharmaceutical, Osaka 567-0878, Japan; ‡Koken Bioscience Institute, Tokyo 115-0051, Japan; and §Department of Biology, School of Education, Waseda University, Tokyo 169-0051, Japan

Edited by Inder M. Verma, The Salk Institute for Biological Studies, La Jolla, CA, and approved July 12, 2005 (received for review March 3, 2005)

Silencing of gene expression by small interfering RNAs (siRNAs) is rapidly becoming a powerful tool for genetic analysis and represents a potential strategy for therapeutic product development. However, there are no reports of systemic delivery for siRNAs toward treatment of bone-metastatic cancer. Accordingly, we report here that i.v. injection of GL3 luciferase siRNA complexed with atelocollagen showed effective reduction of luciferase expression from bone-metastatic prostate tumor cells developed in mouse thorax, jaws, and/or legs. We also show that the siRNA/atelocollagen complex can be efficiently delivered to tumors 24 h after injection and can exist intact at least for 3 days. Furthermore, atelocollagen-mediated systemic administration of siRNAs such as enhancer of zeste homolog 2 and phosphoinositide 3′-hydroxykinase p110-α-subunit, which were selected as candidate targets for inhibition of bone metastasis, resulted in an efficient inhibition of metastatic tumor growth in bone tissues. In addition, up-regulation of serum IL-12 and IFN-α levels was not associated with the *in vivo* administration of the siRNA/atelocollagen complex. Thus, for treatment of bone metastasis of prostate cancer, an atelocollagen-mediated systemic delivery method could be a reliable and safe approach to the achievement of maximal function of siRNA.

bone metastasis | prostate cancer

RNA interference (RNAi) induced by small interfering RNA (siRNA) has recently emerged as a powerful technique that is capable of suppressing expression of individual genes with a high degree of specificity (1). The technique has been used for studies of gene function *in vivo*, primarily in mice. The first demonstration of RNAi-mediated repression in an adult animal showed effective repression of a luciferase reporter gene after hydrodynamic transfection of siRNA expression plasmids into mouse liver (2, 3). Subsequent studies have delivered siRNA by various methods, including viral vector-mediated delivery (4, 5) and lipid-based delivery (6, 7). A more recent study showed that chemically modified siRNAs can silence an endogenous gene after i.v. injection in mice (8). These findings provide hope for using RNAi technology in disease control.

Many studies have used siRNAs as an experimental tool to dissect the cellular pathways that lead to uncontrolled cell proliferation and cancer. To develop siRNAs for cancer therapy, several researchers have investigated them in animal models (9–13). However, reports of RNAi-delivery strategies for bone-metastatic cancer are very limited. For example, in advanced prostate cancer, the sites most frequently affected by metastasis are the bones and regional lymph nodes. Patients with these metastases suffer pain and low limb edema, making it extremely important to explore avenues of treating such bone metastases.

We previously demonstrated the efficacy of atelocollagen for delivery of nucleotides, such as plasmid DNA and antisense oligonucleotides, *in vitro* and *in vivo* (14–19). Recently, we also reported that atelocollagen complexed with siRNA is resistant to nucleases and is efficiently transduced into cells, thereby allowing long-term gene silencing (20). Furthermore, intratumor injection of atelocollagen complexed with siRNA against fibroblast growth factor 4 mRNA showed efficient inhibition of tumor growth in an orthotopic xenograft model of a human nonseminomatous germ cell tumor (20). Another group reported that radiolabeled siRNA mixed with atelocollagen existed in the tumors for at least a week and remained intact and that the vascular endothelial growth factor siRNA with atelocollagen dramatically suppressed tumor angiogenesis and tumor growth in a PC-3 s.c. xenograft model (21). Thus, for local administration of siRNA, an atelocollagen-based nonviral delivery method could be a reliable approach to achieve the maximal function of siRNA *in vivo*. In addition, an atelocollagen complex can be delivered for i.v. injection as nanoparticles, making systemic delivery of siRNA possible. A recent report showed the potential for atelocollagen-mediated systemic antisense therapeutics for treating inflammatory disease (19).

In this study, noninvasive optical imaging technologies were used to facilitate the detection of metastatic lesions and the effects of synthetic siRNAs on tumor regression. The results indicate that systemic administration of atelocollagen complexed with siRNA into a mouse model of bone metastasis demonstrated effective gene silencing and tumor regression in bone-metastatic lesions. Furthermore, we also showed that atelocollagen-mediated systemic delivery of siRNA did not cause any side effects. Thus, systemic delivery of a siRNA/atelocollagen complex may have therapeutic potential in the treatment of advanced prostate cancer with bone metastasis.

Materials and Methods

Atelocollagen. Atelocollagen is a highly purified type I collagen of calf dermis with pepsin treatment (Koken, Tokyo). A collagen molecule has an amino acid sequence called a telopeptide at both N and C termini, which confers most of the collagen's antigenicity. Atelocollagen obtained by pepsin treatment is low in immunogenicity because it is free from telopeptides (22), and it is used clinically for a wide range of purposes, including wound healing and vessel prosthesis and as a bone cartilage substitute and haemostatic agent (16).

Cell Lines. The bioluminescent human prostate carcinoma cell line PC-3M-luc-C6 (Xenogen, Alameda, CA) was cultured in Eagle's minimum essential medium (Invitrogen) supplemented

This paper was submitted directly (Track II) to the PNAS office.

Freely available online through the PNAS open access option.

Abbreviations: siRNA, small interfering RNA; RNAi, RNA interference; EZH2, zeste homolog 2; p110-α, phosphoinositide 3′-hydroxykinase p110-α-subunit.

¶To whom correspondence should be addressed at: Section for Studies on Metastasis, National Cancer Center Research Institute, 1-1, Tsukiji 5-chome, Chuo-ku, Tokyo 104-0045, Japan. E-mail: tochiya@ncc.go.jp.

with 10% heat-inactivated FBS (Equitech-Bio, Kerrville, TX), nonessential amino acids (Sigma-Aldrich), L-glutamine (ICN), 1 mM sodium pyruvate (Sigma-Aldrich), MEM vitamin solution (Sigma-Aldrich), and 200 μg/ml zeocin (Invitrogen). The cells were maintained *in vitro* at 37°C in a humidified atmosphere of 5% CO_2.

siRNA Preparation. Synthetic 21-nt RNAs were purchased from Dharmacon Research (Lafayette, CO) in deprotected, desalted, and annealed form. The sequence for GL3 siRNA is reported in ref. 23. The sequence of human enhancer of zeste homolog 2 (EZH2) siRNA was 5′-GGA AAG AAC GGA AAU CUU AdTdT-3′ and 3′-dTdTC CUU UCU UGC CUU UAG AAU-5′, and human phosphoinositide 3′-hydroxykinase p110-α-subunit (p110-α) siRNA was 5′-GGU UAA AGA UCC AGA AGU AdTdT-3′ and 3′-dTdTC CAA UUU CUA GGU CUU CAU-5′. The nonspecific control siRNA duplex was also purchased from Dharmacon Research.

***In Vivo* Imaging of siRNA Delivery in Mice with Bone-Metastatic Tumors.** Animal experiments in the present study were performed in compliance with the guidelines of the Institute for Laboratory Animal Research at the National Cancer Center Research Institute. Eight- to 9-week-old male athymic nude mice (CLEA Japan, Osaka) were anesthetized by exposure to 1–3% isoflurane on day 0 and subsequent days. On day 0 of the experiments, to generate an experimental metastasis model, the anesthetized animals were injected with 3×10^6 PC-3M-luc-C6 cells suspended in 100 μl of sterile Dulbecco's PBS into the left heart ventricle (24, 25). For *in vivo* imaging, the mice were administered D-luciferin (150 mg/kg, Promega) by i.p. injection. Ten minutes later, photons from animal whole bodies were counted by using the IVIS imaging system (Xenogen) according to the manufacturer's instructions. Data were analyzed by using LIVINGIMAGE 2.50 software (Xenogen). A successful intracardiac injection was indicated by day 0 images that showed a systemic bioluminescence distributed throughout the animal, and only those mice evidencing a satisfactory injection were continued in the experiment. The development of subsequent metastasis was monitored twice a week *in vivo* by bioluminescent imaging.

For preparing the siRNA/atelocollagen complex, equal volumes of atelocollagen (0.1% in PBS at pH 7.4) and siRNA solution were combined and mixed by rotating for 20 min at 4°C. The final concentration of atelocollagen was 0.05%. Four weeks after tumor injection, individual mice (from cohorts containing five animals) were injected with 200 μl of atelocollagen containing 25 μg of luciferase GL3 siRNA, atelocollagen alone, siRNA alone, or nonspecific siRNA/atelocollagen by i.v. tail vein injection. Tumor growth was not affected by these treatments. To control for mouse-to-mouse variability, the bioluminescence ratio for each mouse was normalized by dividing by the 1-day-posttreatment/pretreatment ratio of luciferase intensity for that mouse.

Detection of siRNA in Tumor Tissues or Normal Tissues by RNase Protection Assay. To show siRNA delivery in tumor tissues, 10-week-old male athymic nude mice were inoculated s.c. with 3×10^6 PC-3M-luc-C6 cells suspended in 50 μl of sterile Dulbecco's PBS. After 8 days, when a tumor reached a volume of 50–100 mm^3, tumor-bearing mice (from cohorts containing three animals) were injected with 200 μl of 0.05% atelocollagen containing 25 μg of luciferase GL3 siRNA, atelocollagen alone, or siRNA alone by i.v. tail vein injection. The mice were killed 1 and 3 days after treatment of siRNA/atelocollagen complexes, and total RNA was extracted from a tumor and selected mice tissues by using ISOGEN (Nippon Gene, Tokyo). The RNase protection probe was made with a mirVana microRNA Probe Construction Kit (Ambion, Austin, TX). The cRNA probe specific for the antisense strand of GL3 siRNA was generated by using T7 RNA polymerase and ^{32}P-labeled UTP. Total RNAs were used in an RNase protection assay using the mirVana miRNA Detection Kit (Ambion) per the manufacturer's protocol. Protected fragments were separated by electrophoresis in 15% polyacrylamide 8 M urea gels. The gels were exposed to x-ray films for 30 min, and the films were then scanned and analyzed by using NIH IMAGE software. GL3 siRNA levels were corrected for wet tissue weights.

Atelocollagen-Mediated siRNA Transfection and Tumor Growth Assay *in Vitro*. The EZH2 siRNA or p110-α siRNA complexed with atelocollagen (final concentration = 0.008%) was prefixed to a six-well plate (37.5 pmol of siRNA/250 μl per well) according to the method described in refs. 15 and 20. The cultured PC-3M-luc-C6 cells were plated into the complex-prefixed plate at 5×10^4 cells per well. Bioluminescence from PC-3M-luc-C6 cells highly correlated to the total number of cells (26). For monitoring the inhibition of cell growth, the cells were lysed ($n = 3$) on days 2, 4, and 6 and then analyzed for luciferase activity (Bright-Glo Luciferase Assay System, Promega). Inhibition of luciferase production was normalized to the level of vehicle-treated cells.

Quantitative RT-PCR. Total RNA was extracted from PC-3M-luc-C6 cells by using ISOGEN and treated with DNase I (Takara Shuzo, Otsu, Japan). Five micrograms of total RNA was used to produce cDNAs with oligo(dT) 12 primer by superscript III RNA polymerase (Invitrogen). cDNA was diluted 5-fold and used for quantitative PCR. For quantitation, aliquots of 5 μl of cDNA samples were subjected to quantitative PCR in 50-μl reactions by using Platinum Quantitative PCR SuperMix-UDG (Invitrogen) and Assays-on-Demand TaqMan primers/probe sets (Applied Biosystems) specific for human EZH2, p110-α, and GAPDH. Reactions were carried out by using the Applied Biosystems PRISM 7700 Sequence Detection System. The reactions were incubated at 50°C for 2 min and then heated to 95°C for 2 min, followed by 45 cycles of 30 s at 95°C, 15 s at 60°C, and 20 s at 72°C. Human EZH2 and p110-α expression levels were normalized to GAPDH levels.

Analysis of siRNA/Atelocollagen Treatment for Bone-Metastatic Prostate Cancer. Mice were inoculated with PC-3M-luc-C6 cells into the left cardiac ventricle on day 0 as described above. The EZH2, p110-α, and nonspecific control siRNA (50 μg) with or without 0.05% atelocollagen in a 200-μl volume were injected into the mouse tail vein on days 3, 6, and 9 postinoculation. Each experimental condition included eight animals per group. The development of subsequent metastasis was monitored twice a week *in vivo* by bioluminescent imaging for 4 weeks. To control for mouse-to-mouse variability, the bioluminescence ratio for each mouse was normalized by dividing by the before/after treatment ratio of luciferase intensity for that mouse. At the end of the experiment on day 28, to confirm the presence of neoplastic cells, selected tissues were excised from the mice at necropsy. Tissues were fixed in 4% formaldehyde-PBS(−), embedded in paraffin, cut into 5-mm sections, and stained with hematoxylin/eosin.

Monitoring of IFN Induction in Mice Treated with Atelocollagen-Mediated siRNA. Eight-week-old male athymic nude mice were injected with nonspecific control siRNA (50 μg) with 0.05% atelocollagen in a 200-μl volume by i.v. tail vein injection. Each experimental condition included four animals per group. The positive control group was injected with poly(I:C) (Amersham Pharmacia Biosciences). To measure serum cytokine levels, blood was harvested from mice 2 h after injection by cardiac puncture.

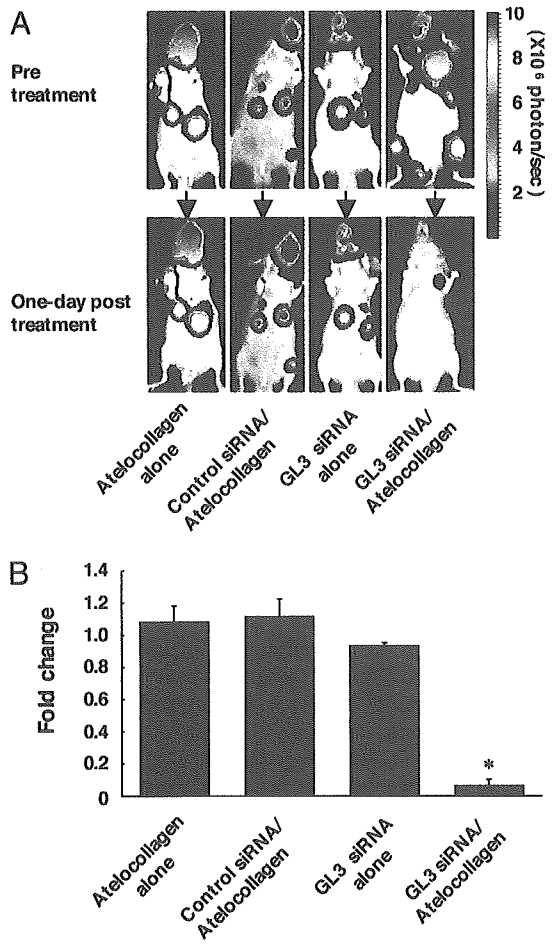

Fig. 1. Monitoring luciferase inhibition *in vivo* with bioluminescent imaging. (*A*) Representative images of nude mice injected with 3×10^6 PC-3M-luc-C6 cells suspended in 100 μl of sterile Dulbecco's PBS into the left ventricle of the heart. Four weeks after tumor injection, each animal was administered i.v. with 200 μl of 0.05% atelocollagen solution, 25 μg of luciferase GL3 siRNA, GL3 siRNA/atelocollagen complex, or nonspecific siRNA/atelocollagen complex. (*B*) Normalized fold change (1 day posttreatment/pretreatment) of bioluminescence emitted from whole body of mice. Data represent the mean ± SD ($n = 4$). *, $P < 0.001$ versus other experimental groups.

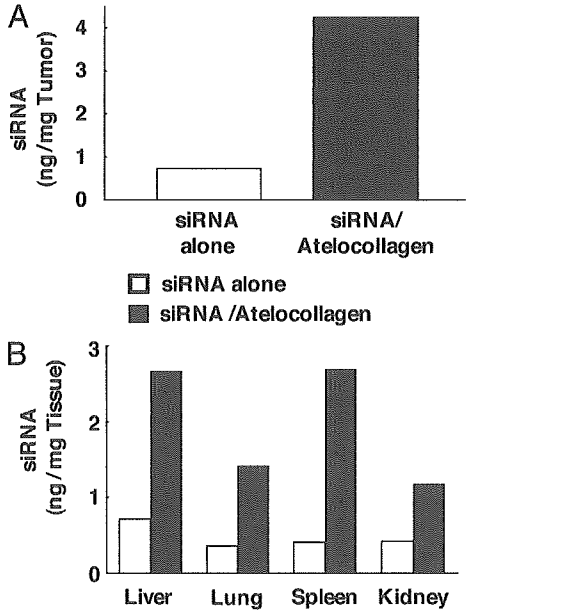

Fig. 2. Distribution of siRNA delivered with atelocollagen in tumor tissues and normal tissues. The nude mice were inoculated s.c. with 3×10^6 PC-3M-luc-C6 cells. Once tumors had reached 50–100 mm^3, tumor-bearing mice were injected with 200 μl of 0.05% atelocollagen containing 25 μg of luciferase GL3 siRNA or siRNA alone by i.v. tail vein injection. The mice were killed 1 day after treatment with siRNA/atelocollagen complexes, and total RNA was extracted from a tumor (*A*) and selected tissues (*B*). Detection of luciferase GL3 siRNA was performed by RNase protection assay. GL3 siRNA levels were corrected for wet tissue weights.

IL-12 (p40) and IFN-α levels (R & D Systems) were measured by ELISA according to the manufacturer's instructions.

Statistical Analysis. The results are given as mean ± SD. Statistical analysis was conducted by using the analysis of variance with the Bonferroni correction for multiple comparisons. $P \leq 0.05$ was considered a significant difference.

Results

Efficient Delivery of Atelocollagen-Mediated Luciferase siRNA in Bone-Metastatic Regions. To increase the potential for bone metastasis from PC-3M-luc-C6 cells, we injected the cells into the left ventricle of the heart (25). Mice with successful intracardiac injection of PC-3M-luc-C6 cells on day 0 were imaged twice a week for up to 4 weeks. In all mice, early indications of metastasis to various tissues were observed within 1 week after cell injection (data not shown). Four weeks after tumor injection, the observed patterns of metastasis indicated lesions developing in the thorax, jaws, and/or legs of the mice (Fig. 1*A*). To test whether atelocollagen-mediated siRNA systemic delivery is valid for a gene silencing effect on the metastatic sites, the animals were treated with atelocollagen alone, a nonspecific control siRNA/atelocollagen complex, a luciferase GL3 siRNA alone, or a luciferase GL3 siRNA/atelocollagen complex i.v. In mice receiving the luciferase siRNA/atelocollagen complex, bioluminescence was inhibited by 80–90% in the whole body, including the bone metastases, when compared with before treatment (Fig. 1). In contrast, the bioluminescent signals of most of the metastatic sites in the mice treated with atelocollagen alone or the control siRNA/atelocollagen complex had increased. Treatment with luciferase siRNA alone either had no effect or slightly suppressed photon emission from the tumor cells. After the imaging analysis, tissues expressing bioluminescence were excised from the mice at necropsy. Subsequent histopathology analysis confirmed micrometastases in the lung, dental pulp, tibia, femur, and other soft tissues (data not shown). Thus, our results indicate that siRNA can be delivered by using atelocollagen and can thereby inhibit gene expression in a specific manner in metastatic sites, including bone metastases.

Enhanced Delivery of siRNA into Tumors by Atelocollagen. The efficacy of delivery of siRNA into tumors was evaluated. Athymic nude mice were inoculated s.c. with 3×10^6 PC-3M-luc-C6 cells and injected i.v. with luciferase siRNA/atelocollagen, luciferase siRNA alone, or atelocollagen alone. We assessed the delivery of siRNA 1 day after the i.v. administration. As shown in Fig. 2*A* and also in Fig. 7, which is published as supporting information on the PNAS web site, a significant amount of siRNA was detected in tumors with atelocollagen-mediated delivery (4.3 ng of siRNA/mg of tumor weight). In contrast, i.v. injection of siRNA alone (0.7 ng/mg of tumor weight) was less efficient compared with atelocollagen-mediated delivery. We also assessed the delivery of luciferase siRNA in several tissues, such as liver, lung, spleen, and kidney. As shown in Fig. 2*B*, a relatively high amount of siRNA was detected in tissues from mice administered with the siRNA/atelocollagen complex com-

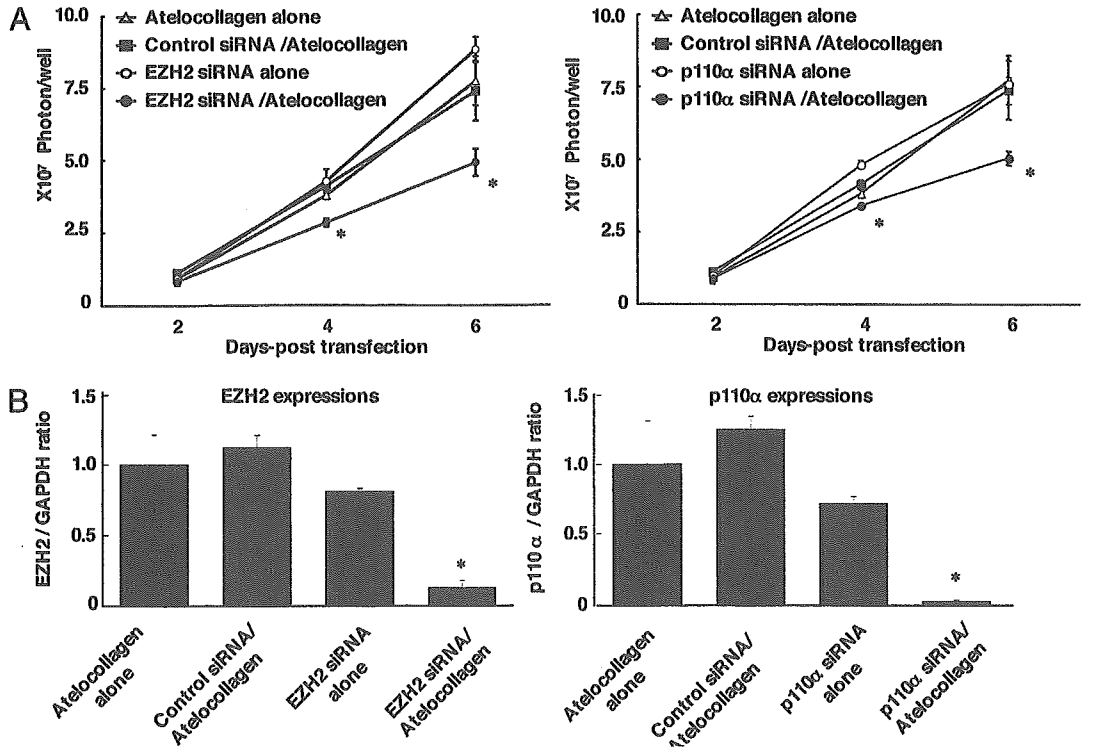

Fig. 3. The EZH2 and p110-α siRNA inhibit PC-3M-luc-C6 cell proliferation and suppress EZH2 and p110-α expression. (*A*) Inhibition of PC-3M-luc-C6 cell proliferation. For monitoring the inhibition of cell growth, cells were lysed on days 2, 4, and 6 and then analyzed for luciferase activity. (*B*) The effects of siRNA transfection on expression of EZH2 and p110-α mRNA. EZH2 and p110-α mRNA expression levels were measured by quantitative PCR. Data represent the mean ± SD ($n = 3$). *, $P < 0.05$ versus cells treated with atelocollagen alone.

pared with mice with siRNA alone. In addition, siRNA delivered with atelocollagen existed intact for at least 3 days (data not shown). Taken together, these results suggest that the systemic injection of the siRNA/atelocollagen complex allows a more efficient delivery of siRNA into tumors than siRNA alone and causes siRNA to be retained for a longer period therein.

Atelocollagen-Mediated siRNA Transfer Allows Efficient Inhibition of PC-3M-luc Cell Growth *in Vitro*. To screen target genes for showing growth inhibition of PC-3M-luc cells, EZH2 and p110-α were selected as target genes. The atelocollagen-mediated siRNA reverse cell transfection method was used. The cultured PC-3M-luc-C6 cells were plated into a siRNA/atelocollagen complex-prefixed plate. For monitoring cell growth, we analyzed luciferase activity. Inhibition of cell growth was observed on PC-3M-luc cells treated with EZH2 and p110-α siRNA/atelocollagen complexes (Fig. 3*A*). Inhibition of mRNA levels of targets was also shown (Fig. 3*B*). These results revealed that EZH2 and p110-α may be the target of inhibition of the metastasis of PC-3M-luc cells.

Inhibition of Metastatic Tumor Growth in Bone Tissues in Animals with Atelocollagen Complex. To assess the inhibition of bone metastasis by the atelocollagen-mediated siRNA delivery system, EZH2 and p110-α siRNA/atelocollagen complexes were administered i.v. into mice on days 3, 6, and 9 of postintracardiac ventricle injection of PC-3M-luc cells. The development of bone metastasis was monitored *in vivo* by bioluminescent imaging. At the end of the experiment on day 28, mice treated with atelocollagen alone and the control siRNA/atelocollagen complex-treated group showed high metastasis in the thorax, jaws, and/or legs (Figs. 4*A* and 5*A*). Total luminescence from all tumors was determined at different times posttreatment for each mouse. As seen in Fig. 4*B*, there was an increase in luminescence in mice treated with atelocollagen alone, the control siRNA/atelocollagen complex, EZH2 siRNA alone, and p110-α siRNA alone, whereas the EZH2 siRNA/atelocollagen-treated and p110-α siRNA/atelocollagen-treated groups had no increase in luminescence during the same observation period. There were significant differences between the EZH2- and p110-α siRNA/atelocollagen-treated groups and the other three experimental groups on day 28 ($P < 0.05$). Histopathological analysis revealed that metastasis of PC-3M-luc-C6 cells in the dental pulp was significantly inhibited by the EZH2 and p110-α siRNA/atelocollagen complexes (Fig. 5*B*). Therefore, the atelocollagen-mediated systemic delivery of siRNA could be a unique strategy for inhibition of bone-metastatic prostate tumor growth *in vivo*.

Absence of IFN Response to Atelocollagen-Mediated siRNA Delivery System. To test whether the atelocollagen-mediated siRNA systemic delivery has the possibility of inducing IFN responses in mice, the plasma levels of IFN-α and IL-12 in mice exposed to the siRNA/atelocollagen complex or poly(I:C) by i.v. injection were measured by ELISA (Fig. 6). As observed with IFN-α and IL-12, the siRNA/atelocollagen complex failed to elicit IFN-α and IL-12 responses, whereas poly(I:C) induced a strong response. These results show that it is possible to administer a siRNA/atelocollagen complex without inducing nonspecific turning on of genes, leading to an immune response.

Discussion

Our findings indicate that siRNA can be delivered to bone-metastatic lesions by atelocollagen-mediated systemic injection. Furthermore, we also showed that an atelocollagen-mediated siRNA delivery system can be used to silence endogenous genes involved in metastatic tumor cell growth.

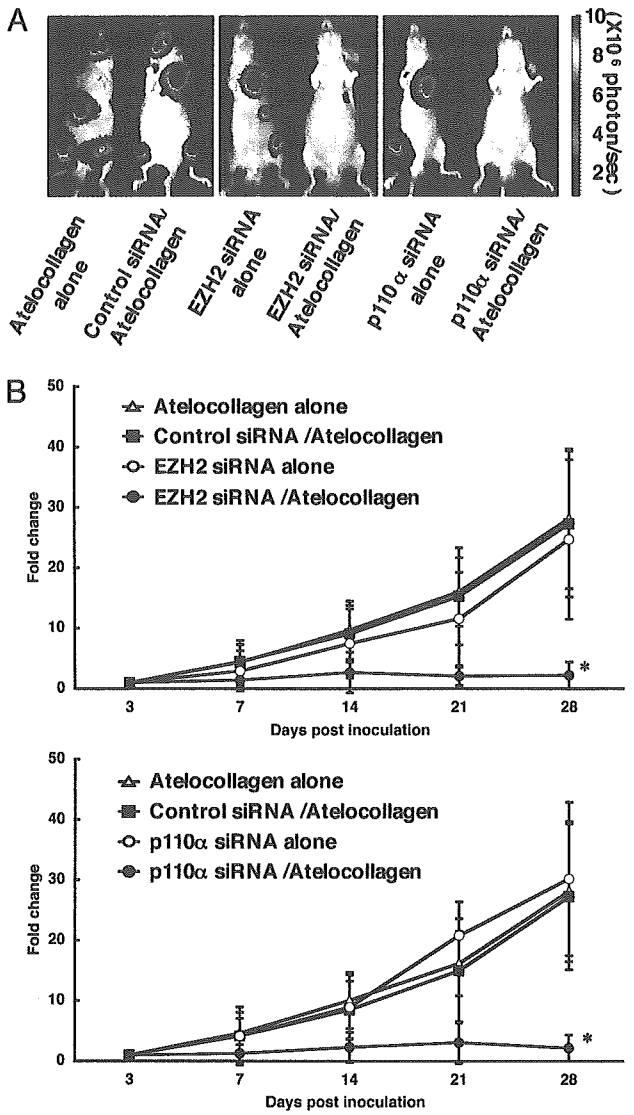

Fig. 4. Inhibition of metastatic tumor growth in bone tissues by the atelocollagen-mediated siRNA delivery system. Mice were inoculated with PC-3M-luc-C6 cells into the left cardiac ventricle on day 0. The EZH2, p110-α, and nonspecific control siRNAs (50 μg) with or without 0.05% atelocollagen in a 200-μl volume were injected into the mouse tail vein on days 3, 6, and 9 postinoculation. Each experimental regimen comprised eight animals. (*A*) Representative images of nude mice at the end of the experiment on day 28. (*B*) Normalized fold change (posttreatment/pretreatment) of bioluminescence emitted from whole body of mice. Data represent the mean ± SD (n = 8). *, $P < 0.05$ versus other experimental groups.

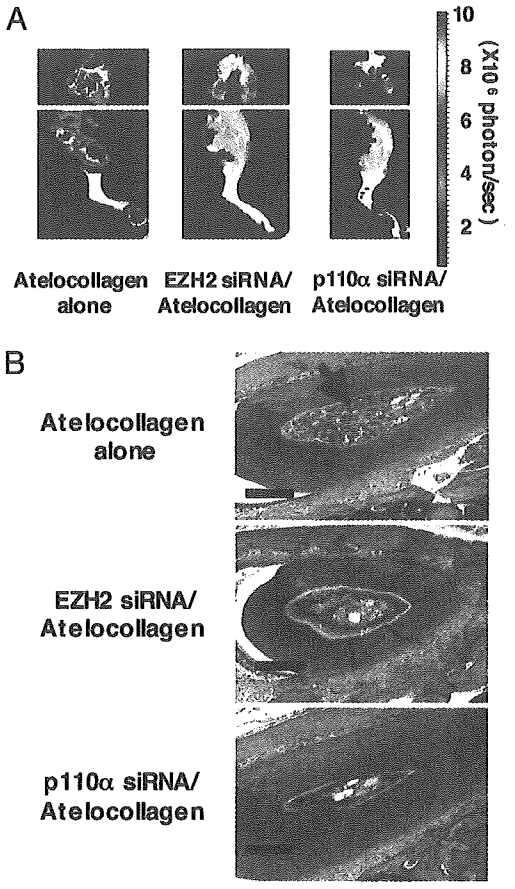

Fig. 5. Confirmation of prostate cancer bone metastasis by *ex vivo* imaging and histopathology. (*A*) The isolated organs from mice (Fig. 4) were reimaged. The bioluminescent signals were detected from the bone region in the jaw and leg of mice treated with atelocollagen alone, EZH2 siRNA/atelocollagen, and p110-α siRNA/atelocollagen, respectively. (*B*) Hematoxylin/eosin-stained sections of the dental pulp from the same mice that were imaged in Fig. 4. Arrow marks the carcinomatous micrometastasis. (Scale bars, 100 μm.)

At present, the main obstacle to the development of therapeutic products using RNAi technologies is a suitable delivery method. Viral delivery systems are efficient but cause concerns over serious side effects (27). Cationic lipid complexes also can be effective siRNA delivery agents (6). However, lipid delivery of synthetic siRNAs can reportedly induce immune activation *in vivo* (28). An important consideration for siRNA-mediated inhibition of gene expression is whether the observed effects are specific and not due to nonspecific "off-target" effects (29) and are free from potential IFN responses (30). Heidel *et al.* (31) showed that it is possible to administer naked, synthetic siRNAs to mice and down-regulate an endogenous or exogenous target without inducing an IFN response. In our experiments, in agreement with Heidel *et al.* (31), injection of siRNA/atelocollagen did not induce an IFN response or IL-12. Therefore, our atelocollagen-based siRNA delivery method can be varied to minimize the potential for an off-target effect of siRNA.

Successful application of RNAi as a therapeutic method requires an efficient and suitable delivery system that can target a restricted cell population *in vivo*. The prolonged circulation time of high-molecular-weight macromolecules enables them to use the vascular abnormalities of solid tumor tissues, a phenomenon called the enhanced permeability and retention (EPR) effect (32, 33). This EPR effect is attributed to anatomical and pathophysiological alterations such as increased vascular density due to neoangiogenesis, impaired lymphatic recovery, and lack of smooth muscle layer in solid tumor vessels. The EPR effect facilitates extravasation of polymeric drugs more selectively at tumor tissues, and this selective targeting to solid tumor tissues may lead to superior therapeutic benefits with fewer systemic adverse effects. In our experiments, siRNA/atelocollagen complexes showed greater selective accumulation in tumor tissues, compared with normal tissues, possibly due to an EPR mechanism. Although further analysis is required, our atelocollagen-mediated siRNA delivery method could possess the potential for selective targeting to tumor tissues.

The major risk faced by patients with prostate cancer is the development of metastatic disease. Although genes associated with metastatic prostate cancer can be identified readily by

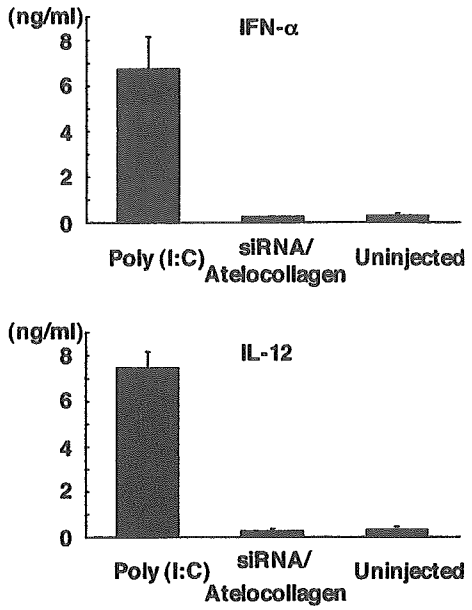

Fig. 6. Absence of IFN response to the atelocollagen-mediated siRNA delivery system. Nude mice were injected with nonspecific control siRNA (50 μg) with 0.05% atelocollagen in a 200-μl volume by i.v. tail vein injection. The positive control group was injected with poly(I:C). Serum was collected 2 h postinjection; IFN-α and IL-12 levels were determined by ELISA. Data represent the mean ± SD (n = 4).

screening techniques [e.g., gene arrays (34)], the validation and characterization of these genes will require sophisticated animal models and gene delivery systems. Expression microarray studies identified EZH2 as a gene overexpressed in hormone-refractory metastatic prostate cancer, and it has been found that patients with clinically localized prostate cancers that express EZH2 have a worse prognosis than those who do not express the protein (34). In addition, knocking down the EZH2 protein in PC3 invasive prostate cancer cells by using RNAi technology inhibited proliferation of cells *in vitro*. In contrast, catalytic subunits of the phosphatidylinositol 3-kinase p110-α regulate a variety of cellular responses such as survival, proliferation, and cell migration (35). In this report, our data demonstrate that expression of EZH2 and p110-α are involved in tumor growth in metastatic osseous sites. It has been reported that EZH2 and p110-α protein are also elevated in breast cancer (36, 37). Therefore, EZH2 and p110-α siRNA/atelocollagen complexes may also have therapeutic potential for inhibiting the growth of breast cancer in bone-metastatic sites. Although EZH2 and p110-α siRNA efficiently inhibited proliferation of PC-3M-luc cells, further work will be required to develop a siRNA therapy that induces the cytocidal effect specific to prostate cancer cells.

In conclusion, we have developed a technique to efficiently and safely deliver siRNA to a bone-metastatic lesion by an atelocollagen-mediated systemic injection and demonstrated specific inhibition of target gene expression. To our knowledge, our results present the first evidence that gene silencing by means of systemic delivery of siRNA/atelocollagen complexes may have therapeutic potential in the treatment of advanced prostate cancer with bone metastasis.

We thank Ms. Ayako Inoue and Ms. Maho Kodama for their excellent technical work. This work was supported in part by a grant-in-aid for the Third-Term Comprehensive 10-Year Strategy for Cancer Control; Health Science Research grants for Research on the Human Genome and Gene Therapy from the Ministry of Health, Labour, and Welfare of Japan; a grant-in-aid for Scientific Research on Priority Areas (Cancer) from the Ministry of Education, Culture, Sports, Science, and Technology; and the Program for Promotion of Fundamental Studies in Health Sciences of the Organization for Pharmaceutical Safety and Research of Japan.

1. Hannon, G. J. & Rossi, J. J. (2004) *Nature* **431,** 371–378.
2. McCaffrey, A. P., Meuse, L., Pham, T. T., Conklin, D. S., Hannon, G. J. & Kay, M. A. (2002) *Nature* **418,** 38–39.
3. Lewis, D. L., Hagstrom, J. E., Loomis, A. G., Wolff, J. A. & Herweijer, H. (2002) *Nat. Genet.* **32,** 107–108.
4. Brummelkamp, T. R., Bernards, R. & Agami, R. (2002) *Cancer Cell* **2,** 243–247.
5. Xia, H., Mao, Q., Paulson, H. L. & Davidson, B. L. (2002) *Nat. Biotechnol.* **20,** 1006–1010.
6. Sorensen, D. R., Leirdal, M. & Sioud, M. (2003) *J. Mol. Biol.* **327,** 761–766.
7. Layzer, J. M., McCaffrey, A. P., Tanner, A. K., Huang, Z., Kay, M. A. & Sullenger, B. A. (2004) *RNA* **10,** 766–771.
8. Soutschek, J., Akinc, A., Bramlage, B., Charisse, K., Constien, R., Donoghue, M., Elbashir, S., Geick, A., Hadwiger, P., Harborth, J., *et al.* (2004) *Nature* **432,** 173–178.
9. Verma, U. N., Surabhi, R. M., Schmaltieg, A., Becerra, C. & Gaynor, R. B. (2003) *Clin. Cancer Res.* **9,** 1291–1300.
10. Filleur, S., Courtin, A., Ait-Si-Ali, S., Guglielmi, J., Merle, C., Harel-Bellan, A., Clezardin, P. & Cabon, F. (2003) *Cancer Res.* **63,** 3919–3922.
11. Duxbury, M. S., Ito, H., Benoit, E., Zinner, M. J., Ashley, S. W. & Whang, E. E. (2003) *Biochem. Biophys. Res. Commun.* **311,** 786–792.
12. Duxbury, M. S., Ito, H., Zinner, M. J., Ashley, S. W. & Whang, E. E. (2004) *Oncogene* **23,** 1448–1456.
13. Spankuch, B., Matthess, Y., Knecht, R., Zimmer, B., Kaufmann, M. & Strebhardt, K. (2004) *J. Natl. Cancer Inst.* **96,** 862–872.
14. Ochiya, T., Takahama, Y., Nagahara, S., Sumita, Y., Hisada, A., Itoh, H., Nagai, Y. & Terada, M. (1999) *Nat. Med.* **5,** 707–710.
15. Honma, K., Ochiya, T., Nagahara, S., Sano, A., Yamamoto, H., Hirai, K., Aso, Y. & Terada, M. (2001) *Biochem. Biophys. Res. Commun.* **289,** 1075–1081.
16. Ochiya, T., Nagahara, S., Sano, A., Itoh, H. & Terada, M. (2001) *Curr. Gene Ther.* **1,** 31–52.
17. Hirai, K., Sasaki, H., Sakamoto, H., Takeshita, F., Asano, K., Kubota, Y., Ochiya, T. & Terada, M. (2003) *J. Gene Med.* **5,** 951–957.
18. Sano, A., Maeda, M., Nagahara, S., Ochiya, T., Honma, K., Itoh, H., Miyata, T. & Fujioka, K. (2003) *Adv. Drug Delivery Rev.* **55,** 1651–1677.
19. Hanai, K., Kurokawa, T., Minakuchi, Y., Maeda, M., Nagahara, S., Miyata, T., Ochiya, T. & Sano, A. (2004) *Hum. Gene Ther.* **15,** 263–272.
20. Minakuchi, Y., Takeshita, F., Kosaka, N., Sasaki, H., Yamamoto, Y., Kouno, M., Honma, K., Nagahara, S., Hanai, K., Sano, A., *et al.* (2004) *Nucleic Acids Res.* **32,** e109.
21. Takei, Y., Kadomatsu, K., Yuzawa, Y., Matsuo, S. & Muramatsu, T. (2004) *Cancer Res.* **64,** 3365–3370.
22. Stenzel, K. H., Miyata, T. & Rubin, A. L. (1974) *Annu. Rev. Biophys. Bioeng.* **3,** 231–253.
23. Elbashir, S. M., Harborth, J., Lendeckel, W., Yalcin, A., Weber, K. & Tuschl, T. (2001) *Nature* **411,** 494–498.
24. Arguello, F., Furlanetto, R. W., Baggs, R. B., Graves, B. T., Harwell, S. E., Cohen, H. J. & Frantz, C. N. (1992) *Cancer Res.* **52,** 2304–2309.
25. Jenkins, D. E., Yu, S. F., Hornig, Y. S., Purchio, T. & Contag, P. R. (2003) *Clin. Exp. Metastasis* **20,** 745–756.
26. Jenkins, D. E., Oei, Y., Hornig, Y. S., Yu, S. F., Dusich, J., Purchio, T. & Contag, P. R. (2003) *Clin. Exp. Metastasis* **20,** 733–744.
27. Scanlon, K. J. (2004) *Anticancer Res.* **24,** 501–504.
28. Sioud, M. & Sorensen, D. R. (2003) *Biochem. Biophys. Res. Commun.* **312,** 1220–1225.
29. Jackson, A. L., Bartz, S. R., Schelter, J., Kobayashi, S. V., Burchard, J., Mao, M., Li, B., Cavet, G. & Linsley, P. S. (2003) *Nat. Biotechnol.* **21,** 635–637.
30. Bridge, A. J., Pebernard, S., Ducraux, A., Nicoulaz, A. L. & Iggo, R. (2003) *Nat. Genet.* **34,** 263–264.
31. Heidel, J. D., Hu, S., Liu, X. F., Triche, T. J. & Davis, M. E. (2004) *Nat. Biotechnol.* **22,** 1579–1982.
32. Greish, K., Fang, J., Inutsuka, T., Nagamitsu, A. & Maeda, H. (2003) *Clin. Pharmacokinet.* **42,** 1089–1105.
33. Satchi-Fainaro, R., Puder, M., Davies, J. W., Tran, H. T., Sampson, D. A., Greene, A. K., Corfas, G. & Folkman, J. (2004) *Nat. Med.* **10,** 255–261.
34. Varambally, S., Dhanasekaran, S. M., Zhou, M., Barrette, T. R., Kumar-Sinha, C., Sanda, M. G., Ghosh, D., Pienta, K. J., Sewalt, R. G., Otte, A. P., *et al.* (2002) *Nature* **419,** 624–629.
35. Katso, R., Okkenhaug, K., Ahmadi, K., White, S., Timms, J. & Waterfield, M. D. (2001) *Annu. Rev. Cell Dev. Biol.* **17,** 615–675.
36. Kleer, C. G., Cao, Q., Varambally, S., Shen, R., Ota, I., Tomlins, S. A., Ghosh, D., Sewalt, R. G., Otte, A. P., Hayes, D. F., *et al.* (2003) *Proc. Natl. Acad. Sci. USA* **100,** 11606–11611.
37. Bachman, K. E., Argani, P., Samuels, Y., Silliman, N., Ptak, J., Szabo, S., Konishi, H., Karakas, B., Blair, B. G., Lin, C., *et al.* (2004) *Cancer Biol. Ther.* **3,** 772–775.

Development and biological analysis of peritoneal metastasis mouse models for human scirrhous stomach cancer

Kazuyoshi Yanagihara,[1,6] Misato Takigahira,[1] Hiromi Tanaka,[1] Teruo Komatsu,[1] Hisao Fukumoto,[5] Fumiaki Koizumi,[5] Kazuto Nishio,[2] Takahiro Ochiya,[3] Yoshinori Ino[4] and Setsuo Hirohashi[4]

[1]Central Animal Laboratory; [2]Pharmacology Division; [3]Section for Studies on Metastasis; [4]Pathology Division, National Cancer Center Research Institute; and [5]Shien-Lab Medical Oncology Department, National Cancer Center Hospital, 5-1-1 Tsukiji, Chuo-ku, Tokyo 104-0045, Japan

(Received February 23, 2005/Accepted March 26, 2005/Online publication June 15, 2005)

The number of published studies on peritoneal dissemination of scirrhous gastric carcinoma is very small as a result of the unavailability of highly reproducible animal models. Orthotopic implantation of HSC-44PE and HSC-58 (scirrhous gastric carcinoma-derived cell lines) cells into nude mice led to dissemination of the tumor cells to the greater omentum, mesenterium, peritoneum and so on, and caused ascites in a small number of animals. Cycles of isolation of the ascitic tumor cells and orthotopic inoculation of these cells were repeated in turn to animals. This was to isolate highly metastatic cell lines with a strong capability of inducing the formation of ascites (44As3 from HSC-44PE; 58As1 and 58As9 from HSC-58). All three cell lines induced tumor formation at the site of orthotopic injection, and caused fatal cancerous peritonitis and bloody ascites in 90–100% of the animals approximately 3–5 weeks after the inoculation. When the parent cells were implanted, the animals became moribund in approximately 12–18 weeks, however, none of the animals developed ascites. Complementary DNA microarray and immunohistochemical analyses revealed differences in the expression levels of genes coding for the matrix proteinase, cell adhesion, motility, angiogenesis and proliferation between the highly metastatic- and parent-cell lines. The usefulness of this model for the evaluation of drugs was assessed by analyzing the stability of the metastatic potential of the cells and the reproducibility. Animals intravenously treated with CPT-11 and GEM showed suppressed tumor growth and significantly prolonged survival. The metastatic cell lines and the *in vivo* model established in the present study are expected to serve as a model of cancerous peritonitis developing from primary lesions, and as a useful means of clarifying the pathophysiology of peritoneal dissemination of scirrhous gastric carcinoma and the development of drugs for its treatment. (*Cancer Sci* 2005; 96: 323–332)

Although therapeutic results for gastric cancer have improved recently, the prognosis of patients with scirrhous gastric carcinoma still remains very poor. Scirrhous gastric carcinoma (diffusely infiltrative carcinoma or Borrmann's type-IV carcinoma, or the linitis plastica-type carcinoma) is characterized macroscopically by rigid thickening of the involved region of the gastric wall, causing it to assume a plate-like appearance, rather than by a well-defined mass.[1] Histopathologically, scirrhous cancer cells do not form glands, but cause diffuse infiltration of a broad region of the gastric wall, resulting in fibrous-like thickening of the gastric wall.[2,3] Because of such pathological features, early clinical diagnosis of scirrhous gastric carcinoma is difficult. By the time the diagnosis is made, peritoneal dissemination or distant metastasis to lymph nodes has already occurred in many cases. Peritoneal dissemination occurs frequently even after radical surgery, and is the cause of death in many patients.[4,5] Thus, peritoneal dissemination, a frequent form of recurrence and metastasis of scirrhous gastric carcinoma, serves as a major factor determining the prognosis of patients with scirrhous gastric carcinoma. To date, however, the mechanism of peritoneal dissemination in this type of cancer has not yet been fully elucidated.

Several theories have been proposed to explain the mechanism of peritoneal dissemination in human gastric cancer; it has been suggested that the cancer cells are detached from the primary lesions and freed into the peritoneal cavity, to colonize the peritoneum and induce cancerous peritonitis. However, most of the proposed theories remain speculations, and are seldom based on adequate evidence.[6–8] It cannot be overemphasized therefore that animal models of this condition are urgently needed to pursue studies on its pathophysiology. Some investigators have reported on a model of this condition established by direct inoculation of cultured gastric cancer cells into the peritoneal cavity.[9,10] It is difficult, however, to view this model as faithfully reflecting the characteristics of cancerous peritonitis observed in clinical cases. In the past, it was considered difficult to reliably establish a model of peritoneal dissemination developing from the primary lesions. Under these circumstances, we established seven cultured cell lines derived from human scirrhous gastric carcinoma and analyzed their characteristics.[11–14] Of these cell lines, the HSC-44PE and HSC-58 cells were found to show spontaneous metastasis to lymph nodes and lungs following s.c. implantation in nude mice.[13,14] Then, to isolate cell lines with a high metastatic potential, we performed repetitive s.c. inoculation of these cell lines and isolated sublines that tended to metastasize to lymph nodes. When these sublines were implanted orthotopically, a small number of animals showed massive bloody ascites. This phenomenon resembled the cancerous peritonitis seen in clinical cases and suggested a high possibility of establishing a reproducible mouse model of peritoneal dissemination.

In the present paper, we shall report on an analysis of the characteristics of tumor cell lines that often cause ascites (cell lines with a high potential for peritoneal dissemination) isolated by repeated orthotopic implantation of HSC-44PE and HSC-58 cells. The paper will also describe the results of cDNA microarray and immunohistochemical analyses of these cell lines as the first step towards clarifying the molecular mechanism of development of peritoneal metastasis in gastric cancer. In addition, the usefulness of these cell lines as a model for drug evaluation will also be discussed.

[6]To whom correspondence should be addressed. E-mail: kyanagih@gan2.res.ncc.go.jp
Abbreviations: cDNA, complementary DNA; CPT-11, camptothecin; GEM, gemcitabine; s.c., subcutaneously; i.p., intraperitoneally; i.v., intravenously.

 doi: 10.1111/j.1349-7006.2005.00054.x

Materials and Methods

Cell lines and culture. HSC-39, HSC-44PE and HSC-58 and cell lines established from human scirrhous gastric carcinomas have been reported previously.[11,14] The cell lines were maintained in RPMI1640 medium (Immuno-Biological Laboratories (IBL), Takasaki, Japan) supplemented with 10% FCS (Sigma Chemical, St. Louis, MO, USA), 100 IU/mL penicillin G sodium and 100 μg/mL streptomycin sulfate (IBL) in a 5% CO_2 and 95% air atmosphere at 37°C. The cells were passaged and expanded by trypsinization (0.05% trypsin and 0.02% EDTA; IBL), followed by replating every 5–7 days. All the cell lines were routinely tested for Mycoplasma by the Central Institute for Experimental Animals (Kawasaki, Japan), and no contamination was detected. For injection into mice, cells in log-phase growth were harvested by trypsinization and washed with serum-free RPMI1640 medium.

Animal experimentation. The animal experimental protocols were approved by the Committee for Ethics of Animal Experimentation, and the experiments were conducted in accordance with the Guidelines for Animal Experiments in the National Cancer Center. The mice were purchased from CLEA Japan (Tokyo, Japan) and maintained under specific pathogen-free conditions. They were provided with sterile food and water and housed in cages. The ambient light was controlled to provide regular 12-h light and 12-h darkness cycles.

Establishment of cell lines with a strong potential for inducing the formation of peritoneal metastasis. HSC-44PE and HSC-58 cell lines were inoculated by the orthotopic implantation technique into BALB/c nude mice. At appropriate intervals, or when moribund, the mice were sacrificed and the ascitic tumor cells were harvested aseptically. The cell suspensions were then cultured *in vitro*. The same procedure was repeated using both cell lines, and cell lines with a high potential for inducing the formation of peritoneal metastasis were established after 12 cycles of stepwise selection. Each resultant cell line after *in vitro* passages 5–10 was used for experiments.

Orthotopic implantation. Six-week-old female BALB/c nude mice were anesthetized by i.p. injection of 2.2.2-tribromoethanol (Aldrich Chemical, Milwaukee, WI, USA) at the dose of 0.28 mg/g bodyweight. Then, after making a small median abdominal incision in the mice under anesthesia, 2×10^6 cells in 0.05-mL volume of RPMI medium were inoculated into the middle wall of the greater curvature of the glandular portion of the stomach using a 30-gauge needle (Nipro, Tokyo, Japan). The stomach was then returned into the peritoneal cavity, and the abdominal wall and skin were closed with an AUTOCLIP applier (Becton-Dickinson, Sparks, MD, USA). The mice were killed 200 days after the tumor cell inoculation or when moribund, and peritoneal dissemination was evaluated by counting the number of tumor nodules in the mesenterium. The body organs were examined for metastasis, and various tissues were processed for histological examination.

Evaluation of the growth rate and metastatic potential of the cell lines. The tumorigenicity and spontaneous-metastatic potential of the cell lines were tested by s.c. injection of $0.5–1 \times 10^7$ cells suspended in 0.2 mL of RPMI1640 medium into 6-week-old female BALB/c nude mice. All the mice were numbered, housed separately, and examined twice weekly for tumor development. The tumor mass was measured in two dimensions with calipers, and the tumor volume was calculated according to the equation $(l \times w^2)/2$ (l = length, w = width). At appropriate intervals or when moribund, the mice were killed, and various organs and tissues were examined for metastasis and processed for histological examination as described.[11]

Therapeutic studies with CPT-11 and GEM. Orthotopic implantation of 2×10^6 44As3 or 58As1 cells was conducted in 6-week-old female BALB/c mice (Day 0). The experimental mice were divided into a control group that received vehicle alone (saline), and experimental groups that received i.v. inoculation of different doses of the drugs (50–200 mg/kg/mouse). On Days 3, 7 and 11, tumor-bearing mice received an i.v. injection of 7-Ethyl-10-[4-(1-piperidino)-1-piperidino] carboxycamptothecin (CPT-11). CPT-11 was purchased from Yakult Honsha (Tokyo, Japan) and dissolved in saline before being injected i.v. Gemcitabine (gemcitabine hydrochloride), chemically characterized as (+)-2′-deoxy-2′, 2′-difluorocytidine monohydrochloride, was purchased from Eli Lilly Japan (Kobe, Japan). The mice were administered i.v. inoculations of GEM on days 3, 7, 10, 14, 17, and 21. Seven mice from each group were killed when moribund, or on Day 70.

Statistical analysis. All the data were expressed as the mean ± SE, and analyzed using the unpaired t-test and a P-value of less than 0.001 was considered to denote statistical significance.

RT-PCR analysis. Total RNA was extracted using the ISOGEN/ISOGEN-LS Poly (A) + Isolation Pack (Nippon Gene, Tokyo, Japan), in accordance with the supplier's protocol. After reverse transcription using 1 μg total RNA with an oligo (dT) primer, the whole mixture was used for PCR detecting human and murine β actin. The primers used were as follows; human β actin forward primer, GGAAATCGTGCGTGACATT; reverse primer, CATCTGCTGGAAGGTGGACAG; murine β actin forward primer, GAAATCGTGCGTGACATCAAA; reverse primer, TACTGGTGCTAGGAGCCA. PCR was performed using an RNA PCR kit (Applied Biosystems, Foster City, CA, USA), under the following conditions; initial denaturation at 95°C for 2 min, 35 cycles of amplification (denaturation at 95°C for 60 s and annealing at 60°C for 60 s), and extension at 72°C for 7 min. The PCR products were electrophoresed on 2% agarose gel, and stained with ethidium bromide.

Gene expression profiling by cDNA microarray analysis. 5 μg total RNA was amplified using an *in vitro* transcription reaction.[15] The amplified RNA (6 μg) was reverse-transcribed using random hexamers and aminoallyl-dUTP. The synthesized cDNA was labeled by allowing it to react with a dye (NHS-ester Cy3 or Cy5, Amersham Biosciences, Buckinghamshire, UK).[16] The labeled cDNA was applied to the DNA microarray (Human IA; Agilent Technologies, Palo Alto, CA, USA) and hybridized at 65°C for 17 h. After washing, the microarray was scanned on a scanner (Agilent, G2565BA) and the image was analyzed using a Feature Extraction software (Agilent). The signal intensity of each spot was calibrated by subtraction from the intensity of the negative control. Global normalization methods were used for identification of the differentially expressed genes in each microarray experiment.

Immunohistochemical Analysis. Mouse antibodies against human Cathepsin L (C2970) and MMP-1 (M6427: Sigma-Aldrich, St. Louis, MO, USA), human VEGF (JH121: Laboratory Vision, Fremont, CA, USA), human EGER (31G7: Zymed Laboratory, San Francisco, CA, USA) and human Smad4 (B-8; Santa Cruz Biotechnology, Santa Cruz, CA, USA) were used for this study. The other antibodies used have been described in a previous study.[14] Immunohistochemical staining was carried out as described previously.[8] The staining was repeated to check for possible technical errors, but the results were consistent. Scores for the expression of various genes were assigned semiquantitatively according to the percentage of the cells stained and the staining intensity.

Results

Establishment of the highly metastatic cell lines. Following s.c. inoculation, 20–40% of the HSC-44PE and HSC-58 cells (cultured scirrhous gastric carcinoma cells) metastasized spontaneously to the regional lymph nodes and lungs. When the subclones isolated by repeated s.c. injection of these cells were implanted orthotopically, they spread to the greater omentum,

 doi: 10.1111/j.1349-7006.2005.00054.x

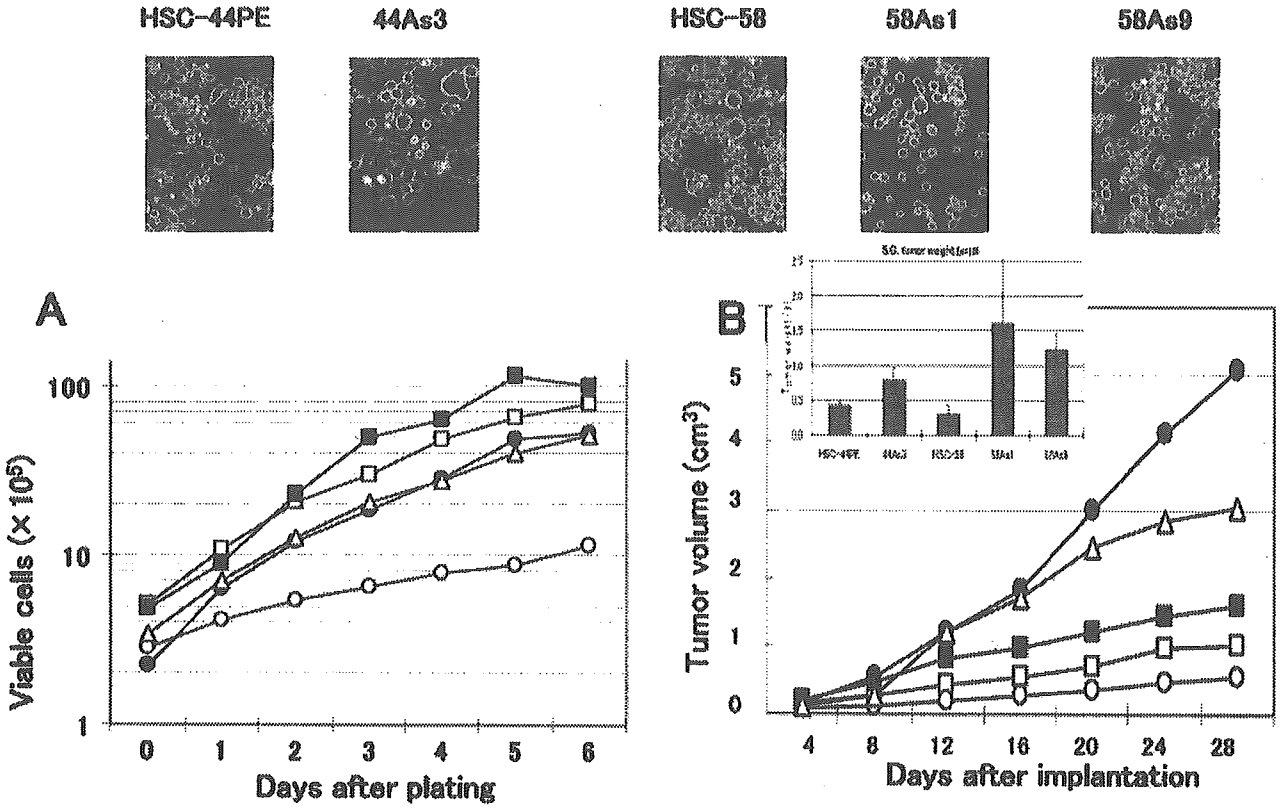

Fig. 1. Phase-contrast micrographs and the growth properties of the sublines showing a high metastatic potential and their parent cell lines. Original magnification, ×200. (A), Growth curves of the cells *in vitro*. Cells were seeded at a density of 1×10^5 cells/well in 6-well plates (Falcon, Lincoln Park, NJ, USA), and the cell numbers were determined daily. The results of a representative experiment are given and the points indicate the average of the results in 3 wells in which the cell numbers varied by 10%. (B), Growth curves of the cells *in vivo*. Tumor volume was measured at predetermined time intervals described in 'Materials and Methods.' HSC-44PE (□), 44As3 (■), HSC-58 (○), 58As1 (●), and 58As9 (△) cell lines were used. Similar results were obtained in a second experiment conducted independently.

mesenterium and so on, and caused the formation of bloody ascites in a small number of animals.[14] Following this result, we incubated the cancer cells isolated from the ascitic fluid of mice, which developed cancerous peritonitis 3–6 months following the orthotopic implantation of HSC-44PE and HSC-58 cells, and attempted orthotopic injection of the incubated cells. This sequence of manipulations was repeated for 12 cycles in an attempt to reliably isolate cell lines that would have higher potentials of undergoing metastasis (in the form of dissemination) over short periods of time. We first obtained a cell line (44As3) from HSC-44PE cells that possessed a high metastatic potential, with a strong capability of inducing ascites. The 44As3 cells resembled the parent HSC-44PE cells in their morphological characteristics. While most cells of this subline exhibited high adhesivity, a small number of spherical cells remained floating and showed proliferative activity. Occasional signet ring cells were also observed (Fig. 1). Although the proliferative potential of the 44As3 cells did not differ greatly from that of the parent cell line *in vitro* (Fig. 1A), the former induced more rapid s.c. tumor formation than the latter (Fig. 1B).

Two highly metastatic cell lines (58As1 and 58As9) were also established from the HSC-58 cells. The 58As1 cells assumed the form of aggregates of spherical cells with low adhesive capacity, which remained floating and showed proliferative activity. In contrast, 58As9 cells often exhibited high adhesivity, resembling the parent cell line, HSC-58, in this characteristic (Fig. 1). Both 58As1 and 58As9 cells exhibited higher proliferative potential *in vitro* than the parent HSC-58 cells (Fig. 1A), and the tumor-forming capability following s.c. injection of these subclones differed markedly from that of the parent cell line; the 58As1 cells, in particular, showed a markedly higher tumor-forming capability (Fig. 1B).

Comparison of the highly metastatic cell lines and the parent cell lines *in vivo*. Table 1 shows the metastatic behavior and the survival days of animals following orthotopic injection of the tumor cells. Orthotopic implantation of 44As3 cells resulted in the formation of bloody ascites approximately 20 days later, and some mice became moribund (Fig. 2D). Dissemination was most often seen to the greater omentum, mesenterium, parietal peritoneum, diaphragm, and so on. Metastasis to the regional lymph nodes and liver was also frequently seen (Table 1). Micrometastasis was observed in the pancreas (also in the lungs, although rarely). The percentage of parent HSC-44PE cells that survived at the site of implantation was 68%. Inoculation of HSC-44PE cells resulted in the animals becoming moribund approximately 85 days after the implantation, but none of the animals developed ascites (Table 1, Fig. 2D).

When 58As1 or 58As9 cells were implanted orthotopically, bloody ascites began to form approximately 3 weeks after the inoculation, accompanied by tumor dissemination to the greater omentum, mesenterium, parietal peritoneum, diaphragm and so on, and the animals died soon thereafter (Table 1, Fig. 2A–C). Lymph node metastasis was observed in all the animals; metastasis to the liver was also noted. Micrometastases were seen in the pancreas and the lungs. Implantation of 58As1 cells was followed by the development of micrometastases in the

Table 1. Metastasis and peritoneal dissemination after orthotopic inoculation of human gastric cancer cell lines and sublines†

Cell line	Survival days	Tumor formation	Ascites	Lymph node	Lung‡	Liver	Pancreas‡	Kidney‡	Disseminated Metastasis			
									Omentum	Mesenterium	Parietal peritoneum	Diaphragm
HSC-44PE	131 ± 44 (85–200)	13/19 (68%)	0/13 (0%)	5/13	0/13	0/13	0/13	0/3	4/13	3/13	2/13	0/13
44As3	33 ± 11 (20–62)	21/21 (100%)	19/21 (90%)	21/21	2/21	19/21	10/21	0/21	21/21	21/21	20/21	14/21
HSC-58	85 ± 16 (68–123)	16/20 (80%)	1/16 (6%)	5/16	1/16	3/16	1/16	0/16	6/16	3/16	3/16	0/16
58As1	32 ± 5 (23–42)	21/21 (100%)	20/21 (95%)	21/21	6/21	19/21	7/21	4/21	21/21	21/21	21/21	13/21
58As9	45 ± 13 (22–68)	14/14 (100%)	14/14 (100%)	14/14	2/14	7/14	1/14	0/14	14/14	10/14	11/14	8/14

†Mice were killed at 200 days after the orthotopic implantation. Data are shown as the number of mice bearing metastasis at the site/total number of mice bearing tumor. ‡Micrometastasis.

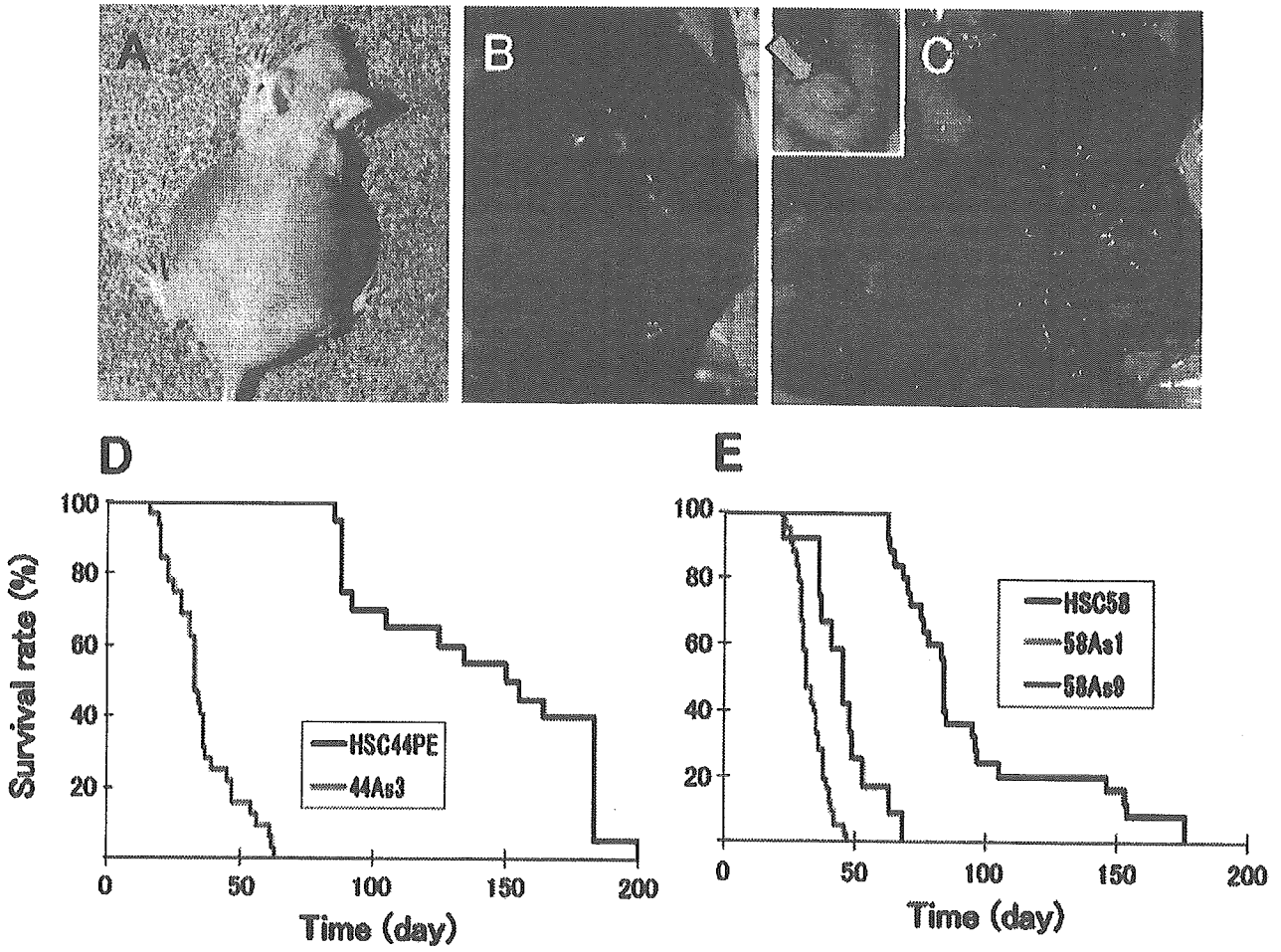

Fig. 2. Macroscopic appearance of the peritoneal disseminations, and survival of nude mice after orthotopic implantation of the cell lines. (A,B), Carcinomatous peritonitis was observed 4 weeks after orthotopic implantation of 58As1 cells. Abdominal distension because of bloody ascites was evident. (C), Peritoneal dissemination was recognized from the innumerable whitish nodules visualized in the abdominal cavity, mesenterium, omentum, parietal peritoneum and diaphragm. Orthotopic implantation of 58As1 cells in the stomach of nude mice was followed by tumor formation 3 weeks later (green arrow, inset). (D), Survival of 44As3-, and HSC-44PE-tumor-bearing mice ($n = 15$; $P < 0.001$). (E), Survival of 58As1-, 58As9-, and HSC-58-tumor-bearing mice ($n = 20$; $P < 0.001$). The experiments were repeated thrice and yielded similar results each time.

 doi: 10.1111/j.1349-7006.2005.00054.x